Electrochimica Acta

Paired electrochemical removal of nitrate and terbuthylazine pesticide from groundwater using mesh electrodes

--Manuscript Draft--

Manuscript Number:	ISE-2020-ELECTACTA-S-21-01231R1
Article Type:	VSI:ISE-2020
Keywords:	Boron-doped diamond anode; Electrochemical oxidation; Electrodenitrification; Groundwater; Iron cathode
Corresponding Author:	Ignasi Sires, Ph.D. Universitat de Barcelona Barcelona, SPAIN
First Author:	Roger Oriol, PhD
Order of Authors:	Roger Oriol, PhD
	Enric Brillas, PhD
	Pere L Cabot, PhD
	José L Cortina, PhD
	Ignasi Sires, Ph.D.
Manuscript Region of Origin:	SPAIN
Abstract:	Groundwater is one of the main freshwater resources on Earth, but its contamination with NO3- and pesticides jeopardizes its viability as a source of drinking water. In this work, a detailed study of single electro-oxidation (EO) and electrodenitrification and paired EO/electrodenitrification processes has been undertaken with simulated and actual groundwater matrices containing 100 mg dm-3 NO3- and/or 5 mg dm-3 terbuthylazine pesticide. Galvanostatic electrolyses were made with 500 cm3 of solutions at pH 4.0-10.5 and 250-100 mA in tank reactors with a RuO2 or boron-doped diamond (BDD) anode and one or two Fe cathodes, all of them in the form of meshes. Most of NO3- removals agreed with a pseudo-first-order kinetics. In Cl--free media, NH4+ predominated as electroreduction product. In chloride media, a greater amount of N-volatiles was determined alongside a slower electrodenitrification, especially with RuO2 due to the partial re-oxidation of electroreduction products like NH4+ by active chlorine. The pesticide decays were also fitted to a pseudo-first order kinetics, and its presence led to a smaller release of N-volatiles. Overall, BDD always favored the pesticide degradation thanks to the action of BDD(OH), whereas RuO2 was preferred for electrodenitrification under some conditions. The EO/electrodenitrification of groundwater was successful once the matrix was softened to minimize its hardness. The NO3- concentration was reduced below the limit established by the WHO. Overall, the BDD/Fe cell was more suitable than the RuO2/Fe cell because it accelerated the pesticide removal with a simultaneous high degree NO3- electroreduction. However, it produced toxic chlorate and perchlorate. A final post-treatment with an anion exchange resin ensures a significant removal of both ions, thus increasing the viability of the electrochemical approach to treat this type of water. Chromatographic analyses revealed the formation of ten heteroaromatic products like desethyl-terbuthylazine and cyanuric acid, alongside oxalic and oxamic as final short-chain carboxylic acids.

Paired electrochemical removal of nitrate and terbuthylazine pesticide from groundwater using mesh electrodes

Roger Oriol[a,1], Enric Brillas[a,1], Pere L. Cabot[a,1], José L. Cortina[b,c], Ignasi Sirés[a,*,1]

[a] *Laboratori d'Electroquímica dels Materials i del Medi Ambient, Departament de Química Física, Facultat de Química, Universitat de Barcelona, Martí i Franquès 1-11, 08028 Barcelona, Spain*

[b] *Chemical Engineering Department, Escola d'Enginyeria de Barcelona Est (EEBE), Universitat Politècnica de Catalunya (UPC)-BarcelonaTECH, Eduard Maristany 10-14, Campus Diagonal-Besòs, 08930 Barcelona, Spain*

[c] *Barcelona Research Center for Multiscale Science and Engineering, Campus Diagonal-Besòs, 08930 Barcelona, Spain*

Paper submitted to be published in ***Electrochimica Acta***

* Corresponding author: Tel.: +34 934039240; fax: +34 934021231.

E-mail address: i.sires@ub.edu (I. Sirés)

[1]Active ISE member

Abstract

Groundwater is one of the main freshwater resources on Earth, but its contamination with NO_3^- and pesticides jeopardizes its viability as a source of drinking water. In this work, a detailed study of single electro-oxidation (EO) and electrodenitrification and paired EO/electrodenitrification processes has been undertaken with simulated and actual groundwater matrices containing 100 mg dm^{-3} NO_3^- and/or 5 mg dm^{-3} terbuthylazine pesticide. Galvanostatic electrolyses were made with 500 cm^3 of solutions at pH 4.0-10.5 and 250-100 mA in tank reactors with a RuO_2 or boron-doped diamond (BDD) anode and one or two Fe cathodes, all of them in the form of meshes. Most of NO_3^- removals agreed with a pseudo-first-order kinetics. In Cl^--free media, NH_4^+ predominated as electroreduction product. In chloride media, a greater amount of N-volatiles was determined alongside a slower electrodenitrification, especially with RuO_2 due to the partial re-oxidation of electroreduction products like NH_4^+ by active chlorine. The pesticide decays were also fitted to a pseudo-first order kinetics, and its presence led to a smaller release of N-volatiles. Overall, BDD always favored the pesticide degradation thanks to the action of BDD($^\bullet$OH), whereas RuO_2 was preferred for electrodenitrification under some conditions. The EO/electrodenitrification of groundwater was successful once the matrix was softened to minimize its hardness. The NO_3^- concentration was reduced below the limit established by the WHO. Overall, the BDD/Fe cell was more suitable than the RuO_2/Fe cell because it accelerated the pesticide removal with a simultaneous high degree NO_3^- electroreduction. However, it produced toxic chlorate and perchlorate. A final post-treatment with an anion exchange resin ensures a significant removal of both ions, thus increasing the viability of the electrochemical approach to treat this type of water. Chromatographic analyses revealed the formation of ten heteroaromatic products like desethyl-terbuthylazine and cyanuric acid, alongside oxalic and oxamic as final short-chain carboxylic acids.

Keywords: Boron-doped diamond anode; Electrochemical oxidation; Electrodenitrification; Groundwater; Iron cathode

1. Introduction

NO_3^- ion and pesticides are the main pollutants of groundwater resources in regions with high density of livestock and agricultural land. The occurrence of these toxic agents is consistently linked to hazardous health problems and diseases exerted on animals and humans, especially in arid and isolated regions where groundwater is a direct source for irrigation and drinking water supply [1]. The application of highly effective water treatment technologies is therefore a must in such cases, aiming to prevent serious health risks. The atmospheric N_xO_y gases, as well as surplus synthetic nitrogen fertilizers and manure spread on land are the main sources of NO_3^- that is further accumulated in groundwater, attaining contents up to 900 mg L^{-1} due to its weak adsorption and high solubility [1,2]. High contents of this anion may cause methaemoglobinaemia and cardiovascular illnesses [3,4], and for this reason, the World Health Organization (WHO) limits to 50 mg L^{-1} its concentration in groundwater intended for human consumption. Classical separation methods such as ion exchange and reverse osmosis are able to remove NO_3^- from water [4], but lately more attention has been drawn to the electrochemical technologies. Among them, electrocoagulation and electrodialysis have been proven effective as separation methods [5], although there is greater interest in transformation treatments involving electroreduction. The latter, which is also called electrodenitrification, consists in the use of an electrocatalytic cathode to increase the activity and/or selectivity of the NO_3^- reduction process. Worth noting, electrodenitrification has been rarely coupled with electrochemical oxidation (EO) [2,4,5-24].

Several factors such as cell configuration, applied current (*I*), solution composition and pH affect the effectiveness of NO_3^- electroreduction. It has been found that this process becomes faster using electrodes with large overpotential for the H_2 evolution reaction (HER), owing to the comparatively slower rate of H^+ and/or H_2O electroreduction. This has been confirmed from the behavior of metallic and semiconductor cathode surfaces made of Pd-Rd [6,7], Sn [8,9], Cu [10,11], Cu-Zn [5,12], stainless steel (SS) [13,14], boron-doped diamond (BDD), SS, graphite, silicon carbide and Pb

[15,16], Sn, Bi, Pb, Al, Zn and In [17], Sn modified Pd [18], Fe, Cu, Ni and carbon foams [19], Cu, Pd, Pt and Rh nanoparticles deposited on reduced graphene [20], Cu-Ni [21], Fe [14,22], TiO_2 nanotubes [23], and Bi-Pd nanoparticles [24]. The electroreduction process is complex and involves the initial transformation of NO_3^- into NO_2^- ion by overall reaction (1), which is subsequently reduced to NH_3 according to reaction (2), via NH_2OH formation, or converted into N_2 gas by reaction (3) through N_xO_y species [2,15,25]:

$$NO_3^- + H_2O + 2e^- \rightarrow NO_2^- + 2OH^- \quad (1)$$

$$NO_2^- + 6H_2O + 6e^- \rightarrow NH_3 + 8OH^- \quad (2)$$

$$2NO_2^- + 4H_2O + 6e^- \rightarrow N_2(g) + 8OH^- \quad (3)$$

EO/electrodenitrification pairing using an undivided reactor appears to be an appealing alternative to increase the viability of the electrochemical technologies, since the typical parasitic oxygen evolution reaction (OER) at the anode (M) is replaced by water conversion to adsorbed hydroxyl radical (M(•OH)) via reaction (4). This is a strong oxidant that can be directly employed to degrade organic pollutants [26-28]:

$$M + H_2O \rightarrow M(^{\bullet}OH) + H^+ + e^- \quad (4)$$

In EO, the non-active BDD anode is more powerful than the active dimensionally stable anodes (DSA®) in chloride-free aqueous matrices because it gives large amounts of physisorbed M(•OH). In contrast, in Cl^- media the oxidation power of DSA® is considerably improved due to its higher selectivity to produce active chlorine (Cl_2/HClO/ClO^-) via reactions (5)-(7) [28,29]. HClO with E^o = 1.36 V prevails at pH 3.0-8.0, whereas at pH > 8.0 the milder ClO^- with E^o = 0.89 V predominates. Once generated, active chlorine can oxidize NH_3 to N_2 from reaction (8) [16,30-33] or to NO_3^- ion from reaction (9) [30,31]. Oxidation of NO_2^- to NO_3^- ion via reaction (10) is feasible [34], thereby reducing the global effectiveness of NO_3^- electroreduction. Active chlorine can be anodically

oxidized to yield toxic and undesired ClO_3^- and ClO_4^- ions [14-16], and the process can be further complicated by the formation of chloramines, initiated by reaction (11) [16,35,36]. Chloramines are preferentially formed in acidic medium and can easily evolve to N_2 or N_2O. Reactions (6)-(11) are homogeneous, thus taking place in the solution bulk. Note that reactions (2), (8), (9) and (11) can involve either NH_3 in alkaline medium or its less reactive protonated form NH_4^+ (pK_a =9.25) in acidic and circumneutral media. In the three latter reactions, NH_3/NH_4^+ reacts with active chlorine in the form of ClO^-/HClO, having the higher or lower redox potential of these oxidants a certain influence on the conversion percentage.

$$2Cl^- \rightarrow Cl_2(aq) + 2e^- \quad (5)$$

$$Cl_2(aq) + H_2O \rightarrow HClO + H^+ + Cl^- \quad (6)$$

$$HClO \leftrightarrows ClO^- + H^+ \qquad pK_a = 7.53 \quad (7)$$

$$2NH_3 + 2ClO^- \rightarrow N_2(g) + 2Cl^- + 2H_2O + 2H^+ + 2e^- \quad (8)$$

$$NH_3 + 4ClO^- \rightarrow NO_3^- + H_2O + H^+ + 4Cl^- \quad (9)$$

$$NO_2^- + ClO^- \rightarrow NO_3^- + Cl^- \quad (10)$$

$$NH_3 + ClO^- \rightarrow NH_2Cl + OH^- \quad (11)$$

Some authors evaluated the influence of the anode material on the NO_3^- electroreduction, showing that in the presence of Cl^-, BDD becomes more efficient than IrO_2-based DSA® [14,16]. This unexpected behavior has been ascribed to the lower adsorption of the products, arising from cathodic NO_3^- reduction, on BDD surface, which drastically diminishes their eventual re-oxidation. Much less is known about the electrodenitrification process in groundwater, although a smaller efficiency could be expected due to different detrimental factors such as the presence of natural organic matter (NOM), the low NO_3^- concentration and the high hardness that can cause the cathode deactivation, thus blocking the electrocatalytic reduction process [25].

In recent years, our group has shown the excellent oxidation power of EO and other electrochemical advanced oxidation processes to destroy pesticides in synthetic solutions [37-42] and even in groundwater [14,29]. A preliminary study about the treatment of the insecticide imidacloprid in groundwater evidenced a better performance of EO/electrodenitrification using Fe as cathode to simultaneously remove the pesticide and NO_3^- ion [14]. However, more research efforts are required to demonstrate the potential viability of paired electrolysis for groundwater remediation in view of the scarce information available so far.

Terbuthylazine (TBZE, CAS number 5915-41-3, $C_9H_{16}ClN_5$, *N-tert*-butyl-6-chloro-*N'*-ethyl-[1,3,5]triazine-2,4-diamine, M = 229.71 g mol^{-1}) belongs to the s-triazine family, and it is one of the most used herbicides in Portugal, Italy and Spain [43]. It is a pollutant of emerging concern because its low solubility in water (about 9 mg dm^{-3} at 20 ºC) and high affinity to soil confer large persistence in surface water, groundwater and marine water, where it has reached 0.2 μg L^{-1}, > 5 μg L^{-1} and 84 ng L^{-1} in EU countries, respectively. Note that 0.1 μg L^{-1} is the recommended maximum content in drinking water, according to EU Directives [43,44]. TBZE is very toxic to living beings at low doses due to its ability to bioaccumulate, posing high long-term risks to non-target plants and soil macroinvertebrates, mammals and aquatic organisms [43]. It is decomposed to desethylterbuthylazine (DE-TBZE), which is also largely persistent in water and even more toxic than the parent herbicide [44]. Several works have reported a large removal of TBZE from water by simple separation methods involving adsorption on membranes [45], selective polymeric materials [46], activated carbon and carbon nanotubes [47] and metal-organic frameworks [48]. Transformation techniques including O_3/activated carbon, solar/O_3 and solar/TiO_2/O_3 [47], UV/H_2O_2 [47,49], UV/TiO_2/chitosan [50] and UV/B-doped TiO_2/O_3 [51] have been tested as well. Tasca et al. [52] used a zero-gap cell equipped with a BDD mesh anode, a RuO_2 mesh cathode and a solid polymer electrolyte, to degrade 300 cm^3 of 4 mg dm^{-3} TBZE in deionized water by EO. About 89% and 97% of pesticide removal was attained

after 60 min at 100 and 500 mA, respectively, with energy consumptions < 11 kWh m^{-3}. Note that the target herbicide possesses 5 N atoms that can be released to contribute to NO_3^- accumulation.

To gain a better insight on the EO/electrodenitrification process, here we report the simultaneous TBZE electrochemical oxidation and NO_3^- electroreduction in actual groundwater matrix. Key experimental parameters like *I* and pH were systematically assessed. The experiments were carried out with an undivided tank reactor equipped with a BDD or RuO_2 (i.e., DSA®-Cl_2) anode and an Fe cathode. Prior to electrolysis with groundwater matrix, the sample was softened to minimize the content of alkaline earth metal ions, a crucial step to avoid the loss of cathode electroactivity upon precipitation of hydroxides and carbonates. Comparative assays were performed with simulated solutions mimicking the anionic composition of the softened groundwater to clarify the evolution of NO_3^- and generated ions and the role of NOM. TBZE was always spiked into the aqueous matrices at a concentration as high as 5.0 mg dm^{-3} in order to minimize the quantification error of all concentrations, thus providing reliable degradation kinetics data. The total nitrogen (TN) concentration decay in solution was monitored as well. A post-treatment with an ion exchange resin was implemented as a final conditioning step to reduce the impact of the oxychlorine anions produced.

2. Materials and methods

2.1. Chemicals

Analytical standards (PESTANAL®) terbuthylazine and desethylterbuthylazine were purchased from Sigma. The solution pH was regulated with analytical grade H_2SO_4 (95-98%) and NaOH (98-100%) purchased from Panreac. Simulated water matrices were prepared with analytical grade electrolytes, including KCl (> 99%) provided by Sigma-Aldrich, and KNO_3 (98%) and K_2SO_4 (99.9%) supplied by Panreac. Other chemicals and solvents used were either of analytical or high-performance liquid chromatography (HPLC) grade provided by Aldrich, Fluka, Lancaster and

Panreac. Ultrapure water (Millipore Milli-Q, > 18.2 MΩ cm) was used to prepare the analytical solutions and simulated water matrices.

2.2. Aqueous matrices

Actual groundwater was collected from a water well located in an agricultural land in the surroundings of Barcelona (Spain). The sample was softened following three consecutive steps: (i) alkalinization up to pH 11.5 by adding 1 M NaOH solution, (ii) sedimentation for 24 h and filtration with regenerated cellulose filter membrane (0.45 μm) to remove the precipitated carbonates and hydroxides and, finally, (iii) acidification with 1 M H_2SO_4 solution to reach the desired pH. The resulting softened groundwater was preserved in a refrigerator at 4 ºC before usage for electrolytic treatments. Table 1 collects the physicochemical parameters of: (i) the raw groundwater; (ii) the softened groundwater once conditioned at pH 4.0 and with TBZE spiked at a concentration of 5.0 mg dm^{-3}; (iii) that softened groundwater, after an electrochemical treatment for 360 min; and (iv) the solution resulting from such electrolysis, after treatment with a Purolite® A532E resin, a polystyrenic strong base anion gel in the chloride form that is recommended by the provider for perchlorate removal. As can be seen, the softening process led to a drastic reduction of the concentration of all alkaline earth metal ions, whereas the Na^+ and SO_4^{2-} concentrations substantially grew up. This sample showed low conductivity and total organic carbon (TOC), whereas its TN content mainly corresponded to NO_3^-. The final post-treatment with the resin allowed the reduction of the ClO_3^-, NO_3^- and SO_4^{2-} concentrations alongside the complete removal of ClO_4^-, with a concomitant increase in the Cl^- content.

Three simulated water samples were prepared to separately assess the behavior of the main anions contained in the softened groundwater. The conductivity of such solutions at neutral pH was around 1.7-1.8 mS cm^{-1} and their composition was: (i) 10 mM K_2SO_4 (980 mg dm^{-3} SO_4^{2-}); (ii) 1.6 mM KNO_3 (100 mg dm^{-3} NO_3^-) + 7.6 mM K_2SO_4 (745 mg dm^{-3} SO_4^{2-}); and (iii) 10 mM KCl (355 mg dm^{-3} Cl^-) + 1.6 mM KNO_3 (100 mg dm^{-3} NO_3^-) + 0.8 mM K_2SO_4 (78 mg dm^{-3} SO_4^{2-}). The pH of

these solutions was adjusted to 4.0, 7.0 and 10.5 and they were electrolyzed, in the absence or presence of 5.0 mg dm^{-3} TBZE, without pH regulation.

2.3. Electrolytic system

The electrolytic assays were performed in an undivided glass tank reactor, which had a jacket to continuously recirculate thermostated water at 25 ºC. Each experiment was made with 500 cm^3 of solution, which was kept under stirring with a magnetic follower at 900 rpm. The anode was either a Nb mesh coated with a 5 µm BDD thin film (3,500 ppm B), purchased from Condias, or a RuO_2 mesh purchased from De Nora, whereas a custom iron mesh (Fe, 99.9%) was used as the cathode. The surface of the anode and cathode immersed into the solution had dimensions of 3.5 cm × 7.5 cm. The electrodes were placed in the center of the tank reactor, separated at a distance of 3 mm. In some cases, two Fe cathodes were used, with the anode sandwiched between them keeping a separation of 3 mm with each cathode. The electrolyses were carried out under galvanostatic conditions with an Amel 2051 potentiostat-galvanostat providing a constant current (*I*) of 250, 500 or 1000 mA. A Demestres 601BR digital multimeter was used to monitor the potential difference between the electrodes. Before each experiment, the Fe cathode was consecutively polished with P240 and P800 sandpapers, submerged in a 20% H_2SO_4 solution, rinsed with Milli-Q water and dried at room temperature.

2.4. Analytical procedures

A Metrohm 644 conductometer and a Crison 2200 pH-meter were used to determine the solution conductance and pH, respectively. A periodic withdrawal of 1.5 cm^3 of treated samples from the tank reactor was made for analysis, followed by filtration with Whatman 0.45 µm PTFE membrane filters.

TN measurements were made with a Shimadzu VCSN TOC analyzer coupled to a TNM-1 unit. The nitrogen mass balance at the end of each assay was made considering the NO_2^-, NO_3^- and NH_4^+ concentrations detected, the solution TN value at each time to account for other soluble N-species and the initial TN of the sample to ascertain the quantity of volatiles released. Free chlorine and total

chlorine contents were obtained by the *N*,*N*-diethyl-*p*-phenylenediamine colorimetric method, using an Unicam UV4 UV/Vis spectrophotometer at λ = 515 nm [53]. The concentration of Cl^-, ClO_3^-, ClO_4^-, NO_2^-, NO_3^- and NH_4^+ ions was obtained following the procedures described elsewhere [54]. The content of iron, calcium, magnesium ions and the other elements in solution was determined by inductively coupled plasma with optical emission spectroscopy (ICP-OES) on a Perkin Elmer Optima 8300 spectrometer.

The TBZE concentration was monitored by reversed-phase HPLC using a Waters 600 liquid chromatograph (LC) coupled to a 996 photodiode array detector. Aliquots of 20 μL were injected into the LC and the separation of organics was achieved by means of a Spherisorb® S5 ODS2 5 μm (150 mm × 4.6 mm (i.d.)) column at 35 ºC, upon elution with a 60:40 (v/v) acetonitrile/water mixture at 1.0 cm^3 min^{-1}. Using Empower® software for control, the peak for TBZE (λ = 222.9 nm) appeared at retention time (t_r) of 7.8 min, with L.O.Q = 0.32 mg dm^{-3} and L.O.D = 0.11 mg dm^{-3}. The peak for DE-TBZE (λ = 214.7 nm) appeared at t_r = 4.1 min, with L.O.Q = 0.59 mg dm^{-3} and L.O.D = 0.19 mg dm^{-3}.

The same LC was equipped with a Bio-Rad Aminex HPX 87H (300 mm × 7.8 mm (i.d.)) column at 35 ºC, its detector selected at λ = 210 and a 4 mM H_2SO_4 solution flowing at 0.6 cm^3 min^{-1} as mobile phase, to quantify the produced acids by ion-exclusion HPLC. The acids detected were oxalic (t_r = 7.3 min), oxamic (t_r = 10.3 min) and cyanuric (t_r = 12.6 min).

The experiments were always made in duplicate, and average results are reported. Figures show the corresponding error bars within a 95% confidence interval.

Solutions of 5.0 mg dm^{-3} TBZE spiked into a simulated water matrix at pH 4.0 and 25 ºC were electrolyzed for 60 min using a BDD/Fe cell at I = 500 mA. The organics were extracted with CH_2Cl_2 (3×50 cm^3). The organic phase was then dried over anhydrous Na_2SO_4, filtered and its volume reduced to ca. 2 cm^3 under N_2 stream for analysis by gas chromatography-mass spectrometry (GC-MS). The analysis was performed by equipping the gas chromatograph with either a polar Agilent

HP-INNOWax GC or a non-polar Teknokroma Sapiens X5-MS column, following the same procedures detailed in earlier work [55]. The mass spectra of heteroaromatic products formed from the initial TBZE degradation were compared with those found in the NIST05 database.

3. Results and discussion

3.1. Electrodenitrification of simulated groundwater without herbicide

A first series of experiments was performed to clarify the effect of pH on the NO_3^- electroreduction, in the absence of pesticide. This was made by electrolyzing 500 cm^3 of solutions with 100 mg dm^{-3} NO_3^- + 7.6 mM SO_4^{2-} at initial pH of 4.0, 7.0 and 10.5 using BDD/Fe and RuO_2/Fe tank reactors at I = 500 mA. Table 2 shows that the acidic and neutral solutions were strongly alkalinized, attaining final pH values of 10.3-10.8 and 10.1-11.2 in the cells with BDD and RuO_2, respectively, as expected from the OH^- generation upon consecutive reduction of NO_3^- to NO_2^-, NH_3 and N_2 via reactions (1)-(3) [14]. The high OH^- content at initial pH 10.5 can explain the small pH variation (± 0.5 units) found in that medium regardless of the anode used (see Table 2).

Fig. 1a presents the variation of NO_3^- concentration with electrolysis time. Using BDD anode, similar decays can be observed at all pH values, with a reduction of 75%-78% at the end of the treatment. This good result can be related to the poor adsorption of the products originated from NO_3^- electroreduction (e.g., NH_4^+ ion) on the BDD surface regardless of the pH. As a result, their subsequent re-oxidation to the parent anion occurred only to a small extent, which was positive in terms of global nitrate removal [15,16]. In contrast, a fluctuating behavior occurred in the cell with RuO_2 anode, with up to 87% of NO_3^- removal at pH 4.0, 81% at pH 10.5 but only up to 56% at pH 7.0. This means that at the latter pH, the products of NO_3^- electroreduction are more largely adsorbed onto the RuO_2 surface, favoring their faster re-oxidation. According to these findings, the use of BDD is more favorable for electrodenitrification at neutral pH, whereas RuO_2 becomes slightly superior in acidic and alkaline media. Fig. 1b depicts that the above concentration decays obeyed a pseudo-first-

order kinetics, and the apparent rate constants ($k(NO_3^-)$) are collected in Table 2. As expected from the trends of Fig. 1, similar $k(NO_3^-)$ values between 4.6×10^{-3} and 5.2×10^{-3} min^{-1} were obtained in the trials with BDD, which rose up to 6.3×10^{-3} min^{-1} for the faster abatement at pH 4.0 using RuO_2.

The accumulated NH_4^+ content increased gradually as the NO_3^- concentration disappeared, as can be seen in Fig. 1c. About 20 mg dm^{-3} as maximal and 12 mg dm^{-3} as minimal of NH_4^+ were finally obtained. A certain TN abatement was found in all the assays, varying between 9.0% and 18%, which can be related to the loss of volatile N-compounds (see Fig. 1d). The speciation of N-containing compounds at the end of all electrolyses shown in Fig. 1e reveals the preeminence of NH_4^+ ion over all the other species, suggesting the leading role of consecutive reactions (1) and (2) in the electrodenitrification process with Fe cathode. The production of volatile N-compounds, like N_xO_y and N_2 via reaction (3) is then a less favorable reduction route. Note that at the final alkaline pH values achieved, the acid/base equilibrium of NH_4^+ ion (pK_a =4.75) results in the accumulation of its conjugated form, which can contribute to the N-volatiles.

Data of Table 2 also show higher average cell potentials (E_{cell}) using BDD, owing to the higher potential required for water discharge as compared to that needed with RuO_2 [26]. The energy consumption (EC) of the process, calculated as $EC = E_{cell}\, I\, t / V$, was then greater for BDD (45.0-50.4 kWh m^{-3} vs 39.0-41.2 kWh m^{-3}).

The above study was extended to a 10 mM Cl^- + 100 mg dm^{-3} NO_3^- + 0.8 mM SO_4^{2-} solution to explore the effect of Cl^- oxidation on the NO_3^- electroreduction. These trials were carried out starting at pH 4.0, 7.0 and 10.5 using both cells at I = 500 mA. In addition, with the BDD anode, the effect of I was studied at pH 4.0. After 360 min, Table 2 shows that final pH values with BDD were similar to those mentioned for chloride-free solutions, whereas they tended to be slightly lower (8.4-10.0) using RuO_2. This behavior suggests that the greater production of active chlorine with the latter anode resulted in a relevant contribution of reactions (9)-(10), eventually leading to a smaller global electrodenitrification with lower OH^- net production from reactions (1)-(3). This hypothesis is

confirmed from the profiles of Fig. 2a, where the NO_3^- concentration decays more slowly using RuO_2. The NO_3^-content was progressively reduced by 79%, 76% and 65% at pH 4.0, 7.0 and 10.5 using BDD, becoming slower until reaching 62%, 60% and 47% removal with RuO_2. Good linear correlations related to a pseudo-first order process were found for all these trends (see Fig. 2b), giving rise to lower $k(NO_3^-)$ values as compared to those determined in the absence of chloride (see Table 2). The loss of efficiency of NO_3^- electroreduction in the chloride medium can be accounted for by the anodic generation of active chlorine (HClO and/or ClO^-) via reactions (5)-(7), which then reacts with NH_4^+ (largely formed from NO_3^- reduction, as shown in Fig. 1c) to originate N_2 gas via reaction (8), regenerate NO_3^- ion via reactions (9) and (10) or produce chloramines via reaction (11). The oxidation of electroreduction products by active chlorine contributed to slow down the global electrodenitrification. Moreover, the progressive deceleration of NO_3^- electroreduction with decrease of $k(NO_3^-)$ was much more remarkable when changing the starting pH from neutral to alkaline (see Fig. 2a and Table 2). This phenomenon can be ascribed to the conversion of HClO to ClO^-, which behaves as a more reactive species, either promoting the oxidation of N-species to NO_3^- or competing with NO_3^- electroreduction. On the other hand, Fig. 2a also shows a more effective electrodenitrification when *I* was increased from 250 to 1000 mA at pH 4.0 using BDD, with the highest NO_3^- removal of 82% attained upon application of the greatest *I*. The corresponding $k(NO_3^-)$ values of Table 2 were upgraded from 3.3×10^{-3} to 6.1×10^{-3} min^{-1} (1.85-fold) upon a 4-fold rise of *I* from 250 to 1000 mA, pointing to a larger influence of NH_4^+ re-oxidation at higher *I*.

The effect of reactions (8)-(11) on electrodenitrification was confirmed by analyzing the evolution of generated NH_4^+ and TN. No NH_4^+ was detected using the RuO_2 anode. Fig. 2c shows that the amount of this ion accumulated in the medium using the BDD anode depended on the applied *I*. While NH_4^+ was not found at 250 mA, it was accumulated between 2.2 and 2.9 mg dm^{-3} at 500 mA and much more largely (up to 10.0 mg dm^{-3}) at 1000 mA, in agreement with the faster NO_3^-

electroreduction. Much larger TN removals were attained in the chloride medium (see Fig. 2d) as compared to those in the chloride-free one (see Fig. 1d), which is explained by the loss of much greater amounts of volatile N-compounds, mainly N_2. For example, up to 65.5% of volatiles was released as maximal at initial pH 7.0 with a BDD anode at 500 mA, much superior to 12.5% found in the absence of chloride. Active chlorine reacts with the generated NH_4^+ via reaction (8), reaching the breakpoint chlorination at a pH at which the HClO and NH_4^+ species have the maximum reactivity, enhancing the production of volatile N-compounds especially at an initial pH of 7.0. At initial pH 10.5, the acid/base equilibrium of NH_4^+ ion (pK_a =9.25) is shifted toward NH_3, the most reactive form with active chlorine, but ClO^- has a lower oxidation power than its acidic counterpart, yielding a lower amount of volatile N-compounds. From these results, the speciation of the final N-compounds is depicted in Fig. 2e. As can be seen, the residual NO_3^- and, more significantly, the volatile N-compounds in most cases were the predominant species. This means that the reduction of NO_3^- to NH_4^+ via reaction (2), followed by the conversion of NH_4^+ to N_2 via reaction (8), are the preferential electrodenitrification steps occurring in the chloride matrix.

Fig. 3a shows the decay of Cl^- concentration for the runs performed in the chloride media. Two trends can be observed: (i) a slow abatement of the ion using RuO_2, achieving close to 47% removal regardless of the pH; and (ii) a faster removal with BDD that was highly dependent on the applied *I*, yielding increasing final removals of 75%, 93% and 96% at 250, 500 and 1000 mA, respectively, at pH 4.0. This agrees with the tendencies of the $k(Cl^-)$ values listed in Table 2 for such assays, obtained from the excellent linear profiles shown in Fig. 3b assuming a pseudo-first-order reaction. The slow Cl^- removal found using RuO_2 is indicative of its main electrodic oxidation via reaction (5). In contrast, its quicker destruction using BDD can be ascribed to the action not only of reaction (5), but also to its reaction with BDD(•OH) originated from reaction (4), which is a more powerful oxidant than RuO_2(•OH). It is noticeable that for BDD, the rise of $k(Cl^-)$ value showed good proportionality with *I*, changing from 3.4×10^{-3} min^{-1} at 250 mA to 1.24×10^{-2} min^{-1} at 1000 mA (see Table 2). This

suggests an almost linear enhancement of the rate of reactions (4) and (5) to destroy the ion. It is well known that further conversion of Cl^- into active chlorine is complicated with BDD due to the subsequent generation of ClO_3^- and ClO_4^- ions as follows [26]:

$$ClO^- + H_2O \rightarrow ClO_2^- + 2H^+ + 2e^- \quad (12)$$

$$ClO_2^- + H_2O \rightarrow ClO_3^- + 2H^+ + 2e^- \quad (13)$$

$$ClO_3^- + H_2O \rightarrow ClO_4^- + 2H^+ + 2e^- \quad (14)$$

The time course of both ions for the same trials is presented in Fig. 3c and 3d. As can be seen, when a RuO_2 anode was used, low ClO_3^- contents up to 120 mg dm^{-3} were always determined at all pH values, whereas no ClO_4^- was found. This behavior indicates that this anode allowed reactions (12) and (13) to some extent, but reaction (14) was completely inhibited. In contrast, much higher ClO_3^- concentrations were found with BDD, thanks to the parallel reaction with BDD($^\bullet$OH). In fact, Fig. 3c shows a similar ClO_3^- evolution at all pH values and a decay of its accumulated content with raising *I* due to its fast reaction with BDD($^\bullet$OH) to obtain much greater amounts of ClO_4^- as the electrolysis was prolonging (see Fig. 3d). For example, at the highest *I* of 1000 mA, a ClO_4^- concentration as high as 925 mg dm^{-3} was determined, being much higher than 35 mg dm^{-3} obtained for ClO_3^- ion. These two ions were the main oxidation products of Cl^- with BDD, since no active chlorine was detected at the end of most treatments.

The similar conductivity of media prepared with and without chloride allowed obtaining an analogous E_{cell} at a given *I*, giving rise to EC values similar to those mentioned above (see Table 2). As expected, E_{cell} and EC increased dramatically with increasing *I*, attaining excessively high values of 13.5 V and 162.0 kWh m^{-3} at 1000 mA, although the higher electrodenitrification power could justify the operation at such high input current.

3.2. Electrochemical oxidation of terbuthylazine in sulfate medium

The oxidation ability of the BDD/Fe cell to remove TBZE from 500 cm^3 of a 10 mM Na_2SO_4 solution with 5.0 mg dm^{-3} herbicide at pH 4.0 by EO was assessed at 500 mA for 360 min. The solution pH slightly increased, whereas the E_{cell} of 8.3 V was analogous to the above matrices with similar conductivity, resulting in an EC close to 50 kWh m^{-3} (see Table 2).

Fig. 4a highlights the fast herbicide abatement with electrolysis time, completely disappearing from the medium in 80 min. Its concentration followed a pseudo-first-order decay, as depicted in the inset of Fig. 4a, with an apparent rate constant k(TBZE) = 9.0×10^{-2} min^{-1}, much greater than that found for Cl^- oxidation (see Fig. 3a and Table 2). This is indicative of a quick reaction of the target herbicide with a constant concentration of BDD($^{\bullet}$OH) formed from reaction (4).

The intermediates and final products formed during the EO process were analyzed as well. The reversed-phase HPLC chromatograms revealed the production of DE-TBZE as main heteroaromatic byproduct. It was rapidly accumulated up to 0.59 mg dm^{-3} at 10 min, further being completely removed in 150 min (see Fig. 4b). Fig. 4c shows that the NH_4^+ concentration grew continuously up to 0.73 mg N dm^{-3}, while NO_3^- was accumulated up to 0.69 mg N dm^{-3}, accounting for a 47.8% and 45.3% of the 1.525 mg N dm^{-3} contained in the herbicide, respectively. This suggests the presence of other more recalcitrant N-products in the final solution, considering the low ability of BDD to produce N_2 (see Fig. 1e). Oxalic, oxamic and cyanuric acids were identified by ion-exclusion HPLC. The two former carboxylic acids are final byproducts that are directly transformed into CO_2, whereas cyanuric acid is the most stable byproduct in the degradation of s-triazines [56]. As can be seen in Fig. 4d, only oxalic acid was completely removed in 120 min, whereas the other acids were very persistent, thereby impeding the overall mineralization of TBZE.

3.3. Electrochemical oxidation/electrodenitrification process in simulated groundwater

The paired EO/electrodenitrification using the BDD/Fe and RuO_2/Fe tank reactors was studied with a 5.0 mg dm^{-3} TBZE + 100 mg dm^{-3} NO_3^- + 7.6 mM SO_4^{2-} solution at pH 4.0 and 500 mA. As in the cases discussed above, the solution pH raised up to ca. 10 after 360 min of electrolysis, the E_{cell}

value was slightly superior with the BDD anode, and EC values were similar to those found without the herbicide (see Table 2). Fig. 5a highlights a much faster TBZE removal using BDD. The herbicide was completely abated in 120 min, a time higher than 80 min needed in sulfate medium (see Fig. 4a), suggesting that the anodic oxidation of NH_4^+ diminishes the amount of BDD(•OH) available for TBZE destruction. In contrast, the herbicide concentration was reduced by 89% using RuO_2, in agreement with the much smaller oxidation power of RuO_2(•OH). This behavior can be confirmed from the corresponding *k*(TBZE) values, which were 9.0-fold higher using BDD (see Table 2). The intermediate DE-TBZE was not detected with this anode, in contrast to that found in sulfate medium (see Fig. 4b), probably because it was accumulated to a smaller amount during the whole electrolysis. This phenomenon did not occur with RuO_2 due to its lower oxidation ability, and DE-TBZE was largely accumulated without apparent destruction, attaining a steady value 1.49 mg dm^{-3} as can be seen in Fig. 5b. The aforementioned behavior can be confirmed from the NO_3^- abatements shown in Fig. 5c. Using the RuO_2 anode, the content decayed with a $k(NO_3^-)$ value of 6.5×10^{-3} min^{-1}. This is similar to that determined in the absence of the herbicide (see Table 2), denoting that EO and electroreduction behave as independent processes using RuO_2. In contrast, the interaction of both processes using BDD caused 0.5-fold drop of $k(NO_3^-)$ in the presence of the herbicide, pointing to the NO_3^- generation during the pesticide degradation. This was confirmed by the fact that in the final solution treated with BDD, small contents of NO_2^- ion were detected alongside a much smaller NH_4^+ accumulation (see Fig. 5d). As in the case of the chloride-free medium without the herbicide, in the presence of this latter pollutant a very low TN removal could be observed (Fig. 5e). Hence, NO_3^- evolved mainly to NH_4^+ via reaction (2) and, to a much smaller extent, to N_2 gas via reaction (3). The speciation of the final N-compounds depicted in Fig. 5f confirms this behavior, showing that the generated NH_4^+ ion and the residual NO_3^- ion were the main N-species regardless of the anode. Note that the N initially contained in the herbicide was not measured with the TN analyzer, but this N (10% of the total TN) appeared gradually as the herbicide byproducts were formed, which justifies the

normalized TN values greater than 1.0 in Fig. 5e. This was more significant using BDD due to its greater power to destroy TBZE.

The study was completed with the case of a simulated matrix with chloride (10 mM Cl^- + 100 mg dm^{-3} NO_3^- + 0.8 mM SO_4^{2-}). TBZE was spiked at a concentration of 5.0 mg dm^{-3}, and the effect of initial pH from 4.0 to 10.5 and applied *I* from 250 to 1000 mA was evaluated with both cells. Comparison of the data of Table 2 for these assays allows concluding that analogous final pH, E_{cell} and EC values were obtained in the absence and presence of TBZE. As expected, the latter two parameters underwent a progressive rise at higher *I*, with the consequent acceleration of all electrodic reactions.

For the cell with the BDD anode, Fig. 6a shows a gradual deceleration of the herbicide disappearance as the pH was risen from 4.0 to 10.5 at each given *I*, with a concomitant longer time needed for total removal. This tendency can also be deduced from the corresponding *k*(TBZE) values collected in Table 2. For example, at 500 mA, the herbicide disappeared after 50, 60 and 100 min at pH 4.0, 7.0 and 10.5, related to decreasing *k*(TBZE) values of 9.9×10^{-2}, 5.7×10^{-2} and 5.2×10^{-2} min^{-1}. Note that at the best pH of 4.0, a slightly quicker herbicide destruction was attained in the presence of chloride, as compared to sulfate medium (*k*(TBZE) = 9.0×10^{-2} min^{-1}) and chloride-free matrix (*k*(TBZE) = 5.7×10^{-2} min^{-1}). This can be explained by its simultaneous reaction with BDD($^\bullet$OH) formed via reaction (4) and active chlorine (HClO) generated via reactions (5) and (6), which accelerated its destruction. The change of this active chlorine form to the weaker oxidant ClO^- can justify the loss of oxidation power when starting at pH 7.0 and 10.5. Fig. 6a also shows that, at each pH, TBZE decayed more rapidly at higher *I*, as result of the greater production of BDD($^\bullet$OH) and active chlorine.

The rate of NO_3^- concentration decay in the chloride medium was slightly lower with the herbicide (see Fig. 6b) than in its absence (see Fig. 2a). This trend can also be established from the lower *k*(NO_3^-) values determined in the former case, listed in Table 2. In the presence of TBZE, part

of the active chlorine oxidizes the organics, yielding additional amounts of NO_3^- ion. This was confirmed by the very low NH_4^+ concentration measured at pH 4.0, which was higher at pH 7.0 and 10.5. Large decays of TN were obtained in the chloride medium with herbicide, as shown in Fig. 6c, in agreement with the discussion in the absence of organics (subsection 3.1). The process was slightly slower at pH 10.5, although large amounts of volatile products (N_2) were always formed. The analysis of the distribution of final N-species shown in Fig. 6d makes in evidence that up to 57% of volatile products were produced, corroborating that reaction (8) becomes the most important step for NO_3^- removal in the presence of Cl^-. However, a smaller proportion of volatile compounds was detected as compared to the chloride matrix without herbicide (see Fig. 2d), owing to the partial loss of active chlorine resulting from its participation in the degradation of the organic molecules.

Fig. 6e reveals that generated active chlorine was rapidly accumulated up to around 90 mg dm^{-3} as maximal, being subsequently destroyed in all cases after 360 min of electrolysis. Only at pH 10.5 some small amounts persisted working at 250 and 500 mA. Although active chlorine attacks the organics and NH_3, with BDD it is mainly destroyed through direct and/or BDD($^\bullet$OH)-mediated oxidation to ClO_3^- and ClO_4^- ions. Fig. 6f shows the rapid formation of ClO_3^- ion, which was more rapidly destroyed at increasing *I* to yield a large amount of the stable ClO_4^- ion (see Fig. 6g). Fig. 6f and 6g highlight that the evolution of both ions only depended on *I*, being quite similar to that determined without organics (see Fig. 3c and 3d).

The results obtained for the EO/electrodenitrification of a solution containing 5.0 mg dm^{-3} TBZE in 10 mM Cl^- + 100 mg dm^{-3} NO_3^- + 0.8 mM SO_4^{2-} using the RuO_2/Fe tank reactor are presented in Fig.7a-7f. Similar trends to those described for the BDD/Fe cell can be observed, but with notable differences that can be ascribed to the smaller ability of RuO_2($^\bullet$OH) to oxidize organics and active chlorine, thus becoming much more effective to remove NO_3^-. Fig.7e reveals the accumulation of much greater contents of active chlorine as compared to the BDD/Fe cell, up to 322 mg dm^{-3} as

maximal, which decreased more largely as *I* grew up. The decay of active chlorine is due to its oxidation to ClO_3^- ion, which is generated to larger extent at higher *I*, as can be seen in Fig. 7f.

Regarding the TBZE abatement using the RuO_2 anode, two tendencies can be observed in Fig. 7a, as compared to the BDD/Fe cell: (i) a lower degradation rate at 250 and 500 mA, with the herbicide being mainly oxidized by $RuO_2(^{\bullet}OH)$, and (ii) a similar degradation at 1000 mA, when larger amounts of active chlorine act as pre-eminent oxidant. The change of *k*(TBZE) between these two regions can be seen in Table 2. It can also be deduced that the best abatements were achieved at pH 4.0, regardless of the applied *I*. The greater production of active chlorine with RuO_2 favors the overall oxidation of NH_3 (not detected) to regenerate more NO_3^- ion at long electrolysis time. This can be inferred by comparing the NO_3^- profiles of Fig. 7b using RuO_2 with those of Fig. 6b using BDD. However, the $k(NO_3^-)$ values of Table 2 are greater for the RuO_2 anode. This is not surprising because they were only determined during the first 60 min of electrolysis, because at higher time the NO_3^- concentration in the medium was practically stabilized due to its fast regeneration from reaction (9). This phenomenon was not found with the BDD anode, where the NO_3^- concentration decayed gradually and excellent linear $\ln([NO_3^-]_0/[NO_3^-])$ vs. *t* plots were obtained up to 300 min of electrolysis. In the same context, Fig. 7c shows a slower TN abatement using RuO_2 than that obtained with BDD (see Fig. 6c). Despite this, high percentages of generated volatile N-compounds were always determined, as highlights Fig. 7d, corroborating again the fast reaction (8) to produce N_2 gas. The main species in final solutions was the residual NO_3^- ion under all operation conditions. No combined chlorine forming chloramines was detected in both cells at the end of any experiment. This suggests that, if produced, they reacted rapidly either with the NO_2^- ion generated from reaction (1) according to reaction (15), or with the active chlorine present in solution to be oxidized to nitrate.

$$NH_2Cl + NO_2^- + H_2O \rightarrow NO_3^- + NH_4^+ + Cl^- \quad (15)$$

3.4. Electrochemical oxidation/electrodenitrification process in softened actual groundwater

Since the cell equipped with BDD yields faster EO and electrodenitrification than that with RuO_2 in chloride matrices, BDD/Fe cells were chosen to study the paired treatment of 5.0 mg dm^{-3} TBZE spiked into actual softened groundwater (100 mg dm^{-3} NO_3^-) conditioned at pH 4.0. One cell had one Fe cathode and was operated at I = 500 mA, whereas another cell had two Fe cathodes sandwiching the BDD anode to work at I = 1000 mA. Moreover, to clarify the influence of NOM on the performance of the system, an assay with the latter cell was carried out with the simulated chloride matrix. A significant effect of using two Fe cathodes instead of one at 1000 mA was the notable decay of E_{cell} (8.8 V vs 14.7 V), giving rise to a great reduction of EC (105.6 kWh m^{-3} vs. 176.4 kWh m^{-3}) (see Table 2). Therefore, the number and position of the electrodes plays a crucial role in the optimization of the energy parameters. In contrast, final pH values close to 10.5 were always obtained at the end of the treatment for both systems.

A similar TBZE content decay can be observed in Fig. 8a for the simulated and actual softened groundwater using two Fe anodes, achieving the total removal in 40 min, which suggests that the influence of NOM oxidation was irrelevant. In fact, Table 2 shows that the k(TBZE) value for both treatments (about 0.16 min^{-1}) was even greater than 0.10 and 0.12 min^{-1} determined for the cell with one Fe cathode at 500 mA (i.e., the same current density than using two Fe cathodes at 1000 mA) and 1000 mA, thus being the TBZE degradation faster and more efficient. In contrast, Fig. 8b depicts a slower destruction of the intermediate DE-TBZE in the actual groundwater after reaching a maximal of 0.26 mg dm^{-3}, which can be ascribed to the loss of oxidizing agents that are partly consumed by NOM. The effect of the organic matter was also evaluated for the evolution of NO_3^-, NH_4^+ and TN. Fig, 8c and 8e show a very fast NO_3^- and TN decay in the simulated groundwater with two Fe cathodes, much more rapid than using one Fe cathode at the same I (see Fig. 6b and 6c). These figures also show a strong inhibition of both parameters in the actual groundwater, which can be explained by the fouling effect of NOM and residual Mg on the cathode surface and a small formation of NO_3^- ion from the degradation of NOM. This influence of the organic matter was also evident for the NO_3^-

content removal when using the cell with one Fe cathode at I = 500 mA to treat the actual groundwater (see Fig. 8c), but it was irrelevant for TN decay as compared to the trial with two Fe cathodes (see Fig. 8e). Fig. 8d reveals the expected greater accumulation of NH_4^+ ion in the three treatments as a greater NO_3^- concentration was abated.

A different behavior was observed for the time course of Cl^-, ClO_3^- and ClO_4^- ions, mainly depending on the applied I and with little influence of the number of Fe cathodes, as can be seen in Fig. 8f-8h. Total Cl^- removal was reached in 240 min using two Fe cathodes, with similar $k(Cl^-)$ values of 1.32-1.40 × 10^{-2} min^{-1}, very close to 1.24 × 10^{-2} min^{-1} determined with one Fe cathode (see Table 2). The lower I of 500 mA with two Fe cathodes yielded an 88% reduction of Cl^- content in 360 min, with $k(Cl^-)$ = 5.7 × 10^{-3} min^{-1}, slightly lower than 7.5 × 10^{-3} min^{-1} found with one Fe cathode (see Table 2). All the active chlorine produced from Cl^- oxidation was then transformed into ClO_3^-, which was converted into ClO_4^-, to larger extent at higher I. For the actual groundwater at I = 1000 mA, 59 mg dm^{-3} of ClO_3^- and 767 mg dm^{-3} of ClO_4^- were finally obtained. The latter content was smaller than 975 mg dm^{-3} determined in the simulated groundwater, which can be due to the loss of active chlorine by reaction with the organic matter. The ClO_3^- and ClO_4^- concentrations after electrolysis of the actual groundwater need to be removed before disposal or reuse. Aiming at evaluating the viability of the technology for future scale-up, a post-treatment was applied by employing a commercial ion-exchange resin. Table 1 shows that this resin allowed the overall removal of ClO_4^- and NO_2^- anions, most of the residual ClO_3^- ion and partial removal of NO_3^- and SO_4^{2-} ions.

3.5. Identification of heteroaromatic byproducts and proposal of initial reaction sequence

Table 3 summarizes the chemical name, molecular structure, type of column, retention time and fragments for the stable heteroaromatic byproducts of TBZE (**1**) identified after 60 min of electrolysis of simulated matrices with and without chloride containing 5.0 mg dm^{-3} herbicide. For this, the

BDD/Fe tank reactor was operated at I = 500 mA. Although different byproducts were identified in each medium due to the different oxidation environments, any organochlorine derivative was found despite the formation and attack of active chlorine in the chloride matrix, as pointed out above. This surprising finding can be explained by the rapid destruction of such chloro-compounds by the strong oxidant BDD(•OH). As can be seen in Table 3, ten heteroaromatics were identified related to: (i) the release of either the Cl atom with hydrogenation (compound **2**) or hydroxylation (compound **3**), the lateral ethyl group (compound **4**), the lateral *tert*-butyl group (compound **6**) or both lateral groups (compound **10**); (ii) the carbonylation of the ethyl group (compounds **5**, **8** and **9**); (iii) the oxidation of the *tert*-butyl group (compound **7**); and (iv) the overall hydroxylation (compound **11**) of these products. Note that compounds **4**-**6** have been previously reported by other authors for **1** degradation [52,57]. Compounds **4** (DE-TBZE) and **11** (cyanuric acid) have been also detected and quantified in this work by reversed-phase and ion-exclusion HPLC, respectively.

Based on the identified heteroaromatics, an initial route for **1** destruction by EO with a BDD anode is proposed in Fig. 9. In this pathway, BDD(•OH) is assumed as the main oxidant. The initial attack of this radical over **1** leads to 5 compounds: (i) **2** with hydrogenation and Cl loss, (ii) **3** with hydroxylation and Cl release, (iii) **4** with release of the ethyl group, (iv) **5** with carbonylation of the ethyl group and (v) **6** with loss of the *tert*-butyl group. The subsequent release of the ethenyl group with oxidation of the *tert*-butyl group of **3** yields **7**, whereas the hydroxylation of **5** gives **8** and the carbonylation of **6** produces **9**. Transformation of **5** and **8** into **4**, as well as that of **5** into **9**, is feasible. Compounds **4**-**6**, **8** and **9** can then evolve to **10** and all products to **11** as final heteroaromatic.

4. Conclusions

This study has presented a comprehensive set of EO, electroreduction and EO/electroreduction trials in simulated and actual groundwater matrices with only NO_3^-, only TBZE or NO_3^- + TBZE, in the absence and presence of Cl^-. The BDD/Fe and RuO_2/Fe cells showed a very high effectiveness to

simultaneously remove nitrate and pesticide from the solutions. From our results, it can be concluded that an effective treatment of groundwater polluted with nitrate and TBZE pesticide requires a sequence of three steps: (i) Softening to minimize the Ca^{2+} and Mg^{2+} content that block the electocatalytic nitrate electroreduction; (ii) EO/electrodenitrification with a BDD/Fe or RuO_2/Fe cell, preferably with two Fe cathode because the greater exposed surface favored the occurrence of electrocatalysis; and (iii) post-treatment with an anion-exchange resin to minimize the chlorate and perchlorate concentrations and achieve an additional nitrate removal. The NOM contained in the groundwater had no negative influence on TBZE removal, but it decelerated the nitrate removal. All removals became faster as the applied current was increased from 250 to 1000 mA. Once demonstrated that the paired electrolysis of nitrate + pesticide solutions can be highly effective with BDD/Fe and RuO_2/Fe cells at small scale, further work is being carried out in our laboratory to scale-up the treatment using a flow reactor.

Acknowledgements

The authors thank the financial support from project PID2019-109291RB-I00 (AEI, Spain). R. Oriol acknowledges the FPI grant awarded by MINECO (Spain).

References

[1] M. Gutiérrez, R.N. Biagioni, M.T. Alarcón-Herrera, B.A. Rivas-Lucero, An overview of nitrate sources and operating processes in arid and semiarid aquifer systems, Sci. Total Environ. 624 (2018) 1513–1522.

[2] M. Duca, M.T.M. Koper, Powering denitrification: the perspectives of electrocatalytic nitrate reduction, Energy Environ. Sci. 5 (2012) 9726–9742.

[3] M. Zhou, W. Fu, H. Gu, L. Lei, Nitrate removal from groundwater by a novel three-dimensional electrode biofilm reactor, Electrochim. Acta 52 (2007) 6052–6059.

[4] M. Shrimali, K.P. Singh, J. Greeley, New methods of nitrate removal from water, Environ. Poll. 112 (2001) 351–359.

[5] M. Li, C. Feng, Z. Zhang, X. Lei, R. Chen, Y. Yang, N. Sugiura, Simultaneous reduction of nitrate and oxidation of by-products using electrochemical method, J. Hazard. Mater. 171 (2009) 724–730.

[6] H. Cheng, K. Scott, P.A. Christensen, Paired electrolysis in a solid polymer electrolyte reactor-simultaneously reduction of nitrate and oxidation of ammonia, Chem. Eng. J. 108 (2005) 257–268.

[7] H. Cheng, K. Scott, P.A, Christensen, Application of a solid polymer electrolyte reactor to remove nitrate ions from wastewater, J. Appl. Electrochem. 35 (2005) 551–560.

[8] I. Katsounaros, G. Kyriacou, Influence of the concentration and the nature of the supporting electrolyte on the electrochemical reduction on tin cathode, Electrochim. Acta 52 (2007) 6412–6420.

[9] I. Katsounaros, G. Kyriacou, Influence of nitrate concentration on its electrochemical reduction on tin cathode: identification of reaction intermediates, Electrochim. Acta 53 (2008) 5477–5484.

[10] D. Reyter, D. Bélanger, L. Roué, Study of the electroreduction of nitrate on copper in alkaline solution, Electrochim. Acta 53 (2008) 5977–5984.

[11] W. Huang, M. Li, B. Zhang, C. Feng, X., Lei, B. Xu, Influence of operating conditions on electrochemical reduction of nitrate in groundwater, Water Environ. Res. 85 (2013) 224–231.

[12] M. Li, C. Feng, Z. Zhang, Z. Shen, N. Sugiura, Electrochemical reduction of nitrate using various anodes and a Cu/Zn cathode, Electrochem. Commun. 11 (2009) 1853–1856.

[13] B. Talhi, F. Monette, A. Azzouz, Effective and selective nitrate electroreduction into nitrogen through synergistic parameter interactions, Electrochim. Acta 58 (2011) 276–284.

[14] R. Oriol, M.P. Bernícola, E. Brillas, P.L. Cabot, I. Sirés, Paired electrooxidation of insecticide imidacloprid and electrodenitrification in simulated and real water matrices, Electrochim. Acta 317 (2019) 753–765.

[15] E. Lacasa, P. Cañizares, J. Llanos, M.A. Rodrigo, Effect of the cathode material on the removal of nitrates by electrolysis in non-chloride media, J. Hazard. Mater. 213-214 (2012) 478–484.

[16] E. Lacasa, J. Llanos, P. Cañizares, M.A. Rodrigo, Electrochemical denitrificacion with chlorides using DSA and BDD anodes, Chem. Eng. J. 184 (2012) 66–71.

[17] M. Dortsiu, I. Katsounaros, C. Polatides, G. Kyriacou, Influence of the electrode and the pH on the rate and the product distribution of the electrochemical removal of nitrate, Environ. Technol. 34 (2013) 373–381.

[18] Y.Y. Birdja, J. Yang, M.T.M. Koper, Electrocatalytic reduction of nitrate on tin-modified palladium electrodes, Electrochim. Acta 140 (2014) 518–524.

[19] L. Rajic, D. Berroa, S. Gregor, S. Elbakri, M. MacNeil, A.N. Alshawabkeh, Electrochemically-induced reduction of nitrate in aqueous solution, Int. J. Electrochem. Sci, 12 (2017) 5998–6009.

[20] C. Sun, F. Li, H. An, Z. Li, A.M. Bond, J. Zhang, Facile electrochemical co-deposition of metal (Cu, Pd, Pt, Rh) nanoparticles on reduced graphene oxide for electrocatalytic reduction of nitrate/nitrite, Electrochim. Acta 269 (2018) 733–741.

[21] Y. Zhang, Y. Zhao, Z. Chen, L. Wang, P. Wu, F. Wang, Electrochemical reduction of nitrate via Cu/Ni composite cathode paired with Ir-Ru/Ti anode: high efficiency and N_2 selectivity, Electrochim. Acta 291 (2018) 151–160.

[22] L. Wu, Y. Shi, C. Su, H. Cao, G. Zheng, Efficient electrochemical reduction of high concentration nitrate by a stepwise method, Catal. Lett. 149 (2019) 1216–1223.

[23] D.E. Kim, D. Pak, Ti plate with TiO_2 nanotube arrays as a novel cathode for nitrate reduction, Chemosphere 228 (2019) 611–618.

[24] I. Sanjuán, L. García-Cruz, J. Solla-Gullón, E. Expósito, V. Montiel, Bi-Sn nanoparticles for electrochemical denitrification: activity and selectivity towards N_2 formation, Electrochim. Acta 340 (2020) 135914.

[25] J. Martínez, A. Ortiz, I. Ortiz, State-of-the-art and perspectives of the catalytic and electrocatalytic reduction of aqueous nitrates, Appl. Catal. B: Environ. 207 (2017) 42–59.

[26] J.R. Steter, E. Brillas, I. Sirés, On the selection of the anode material for the electrochemical removal of methylparaben from different aqueous media, Electrochim. Acta 222 (2016) 1464–1474.

[27] S. Lanzalaco, I. Sirés, A. Galia, M.A. Sabatino, C. Dispenza, O. Scialdone, Facile crosslinking of poly(vinylpyrrolidone) by electro-oxidation with IrO2-based anode under potentiostatic conditions, J. Appl. Electrochem. 48 (2018) 1343–1352.

[28] G. Daniel, Y. Zhang, S. Lanzalaco, F. Brombin, T. Kosmala, G. Granozzi, A. Wang, E. Brillas, I. Sirés, C. Durante, Chitosan-derived nitrogen-doped carbon electrocatalyst for a sustainable upgrade of oxygen reduction to hydrogen peroxide in UV-assisted electro-Fenton water treatment, ACS Sustain. Chem. Eng. 8 (2020) 14425–14440.

[29] R. Oriol, D. Clematis, E. Brillas, J.L. Cortina, M. Panizza, I. Sirés, Groundwater treatment using a solid polymer electrolyte cell with mesh electrodes, ChemElectroChem 6 (2019) 1235–1243.

[30] L. Li, Y. Liu, Ammonia removal in electrochemical oxidation: mechanism and pseudo-kinetics, J. Hazard. Mater 161 (2009) 1010–1016.

[31] G. Pérez, J. Saiz, R. Ibañez, A.M. Urtiaga, I. Ortiz, Assessment of the formation of inorganic oxidation by-products during the electrocatalytic treatment of ammonium from landfill leachates, Water Res. 46 (2012) 2579–2590.

[32] C. Zhang, D. He, J. Ma, D. Waite, Active chlorine mediated ammonia oxidation revisited: reaction mechanism, kinetic modelling and implications, Water Res. 145 (2018) 220–230.

[33] P. Mandal, M.K. Yadav, A.K. Gupta, B.K. Dubey, Chlorine mediated indirect electro-oxidation of ammonia using non-active PbO_2 anode: influencing parameters and mechanism identification, Sep. Purif. Technol. 247 (2020) 116910.

[34] D.G. Wahman, G.E. Speitel Jr, Relative importance of nitrite oxidation by hypochlorous acid under chloramination conditions, Environ. Sci. Technol. 46 (2012) 6056–6064.

[35] J. Chen, H. Shi, J. Lu, Electrochemical treatment of ammonia in wastewater by RuO_2-IrO_2-TiO_2/Ti electrodes, J. Appl. Electrochem. 37 (2007) 1137–1144.

[36] A. Kapalka, A. Katsaounis, N.L. Michels, A. Leonidova, S. Souentie, C. Comninellis, K.M. Udert, Ammonia oxidation to nitrogen mediated by electrogenerated active chlorine on Ti/PtOx-IrO_2, Electrochem. Commun. 12 (2010) 1203–1205.

[37] I. Sirés, E. Brillas, G. Cerisola, M. Panizza, Comparative depollution of mecoprop aqueous solutions by electrochemical incineration using BDD and PbO_2 as high oxidation power anodes, J. Electroanal. Chem. 613 (2008) 151–159.

[38] A.R.F. Pipi, I. Sirés, A.R. De Andrade, E. Brillas, Application of electrochemical advanced oxidation processes to the mineralization of the herbicide diuron, Chemosphere 109 (2014) 49–55.

[39] F. Gozzi, I. Sirés, A. Thiam, S.C. de Oliveira, A, Machulek Jr., E. Brillas, Treatment of single and mixed pesticide formulations by solar photoelectro-Fenton using a flow plant, Chem. Eng. J. 310 (2017) 503–513.

[40] D.R.V. Guelfi, F. Gozzi, A. Machulek Jr., I. Sirés, E. Brillas, S.C. de Oliveira, Degradation of herbicide S-metolachlor by electrochemical AOPs using a boron-doped diamond anode, Catal. Today 313 (2018) 182–188.

[41] D.R.V. Guelfi, E. Brillas, F. Gozzi, A. Machulek Jr., S.C. de Oliveira, I. Sirés, Influence of electrolysis conditions on the treatment of herbicide bentazon using artificial UVA radiation and sunlight. Identification of oxidation products, J. Environ. Manage. 231 (2019) 213–221.

[42] D.R.V. Guelfi, Z. Ye, F. Gozzi, S.C. de Oliveira, A. Machulek Jr., E. Brillas, I. Sirés, Ensuring the overall combustion of herbicide metribuzin by electrochemical advanced oxidation processes. Study of operation variables, kinetics and degradation routes, Sep. Purif. Technol. 211 (2019) 637–645.

[43] A.L. Tasca, M. Puccini, A. Fletcher, Terbuthylazine and desethylterbuthylazine: recent occurrence, mobility and removal techniques, Chemosphere 202 (2018) 94–104.

[44] P. Bottoni, P. Grenni, L. Lucentini, A. Barra Caracciolo, Terbuthylazine and other triazines in Italian water resources, Microchem. J. 108 (2013) 136–142.

[45] E. Drazevic, K. Kosutic, S. Fingler, V. Drevenkar, Removal of pesticides from the water and their adsorption on the reverse osmosis membranes of defined porous structure, Des. Water Treat. 1-3 (2011) 161–170.

[46] S. Ronka, M. Kujawska, H. Juskiewicz, Triazines removal by selective polymeric adsorbent, Pure Appl. Chem. 11 (2014) 1755–1769.

[47] P.M. Álvarez, D.H.. Quiñones, I. Terrones, A. Rey, F.J. Beltrán, Insights into the removal of terbuthylazine from aqueous solution by several treatment methods, Water Res. 98 (2016) 334–343.

[48] L. Liang, X. Wang, Y. Sun, P. Ma, X. Li, H. Piao, Y. Jiang, D. Song, Magnetic solid-phase extraction of triazine herbicides from rice using metal-organic framework MIL-101(Cr) functionalized magnetic particles, Talanta 179 (2018) 512–519.

[49] S. Sorlini, F. Gialdini, M. Stefan, UV/H_2O_2 oxidation of arsenic and terbuthylazine in drinking water, Environ. Monit. Assess. 186 (2014) 1311–1316.

[50] A.F. Tchicaya, S.B. Wognin, I.A.A. Aka, Y.M. Kouassi, A.L.M. N'Guessan, Photocatalytic degradation of the herbicide terbuthylazine: preparation, characterization and photoactivity of the immobilized thin layer of TiO_2/chitosan, J. Photochem. Photobiol. A 309 (2015) 22–29.

[51] D.H. Quiñones, A. Rey, P.M. Álvarez, F.J. Beltrán, G.L. Puma, Boron doped TiO_2 catalysts for photocatalytic ozonation of aqueous mixtures of common pesticides: diuron, o-phenylphenol, MCPA and terbuthylazine, Appl. Catal. B: Environ. 178 (2015) 74–81.

[52] A.L. Tasca, M. Puccini, D. Clematis, M. Panizza, Electrochemical removal of terbuthylazine: boron-doped diamond anode coupled with solid polymer electrolyte, Environ. Pollut. 251 (2019) 285–291.

[53] APWA, AWWA, WEF, Standard Methods for the Examination of Water and Wastewater, 21st ed., Method Number 4500-Cl Chlorine (residual)–G. DPD Colorimetric Method, American Public Health Association, Washington D.C., 2005, pp. 4-67 and 4–68.

[54] A. Thiam, I. Sirés, J.A. Garrido, R.M. Rodríguez, E. Brillas, Effect of anions on electrochemical degradation of azo dye Carmoisine (Acid Red 14) using a BDD anode and air-diffusion cathode, Sep. Purif. Technol. 140 (2015) 43–52.

[55] J.R. Steter, E. Brillas, I. Sirés, Solar photoelectro-Fenton treatment of a mixture of parabens spiked into secondary treated wastewater effluent at low input current, Appl. Catal. B: Environ. 224 (2018) 410–418.

[56] N. Borràs, R. Oliver, C. Arias, E. Brillas, Degradation of atrazine by electrochemical advanced oxidation process using boron-doped diamond anode, J. Phys. Chem. 114 (2010) 6613–6621.

[57] S.V. Pereira, T. Reis, B.S. Souza, R.F. Dantas, D.A. Azevedo, M. Dezotti, C. Sans, S. Esplugas, Oestrogenicity assessment of s-triazines by products during ozonation, Environ. Technol. 36 (2014) 1-25.

Figure captions

Fig. 1. (a) NO_3^- concentration removal during the electrodenitrification of 500 cm^3 of a solution containing 100 mg dm^{-3} NO_3^- + 7.6 mM SO_4^{2-} in ultrapure water at initial pH 4.0, 7.0 and 10.5, using undivided stirred BDD/Fe or RuO_2/Fe tank reactors at 500 mA and 25 ºC. (b) Pseudo-first-order kinetic analysis of trends of plot (a), (c) accumulated NH_4^+ contents, (d) normalized total nitrogen decays, and (e) percent distributions of the nitrogen species at the end of the trials.

Fig. 2. (a) NO_3^- content decay during the electrodenitrification of 500 cm^3 of a solution containing 10 mM Cl^- + 100 mg dm^{-3} NO_3^- + 0.8 mM SO_4^{2-} in ultrapure water at different pH values, using undivided stirred BDD/Fe or RuO_2/Fe tank reactors at several *I* values and 25 ºC. (b) Pseudo-first-order kinetic analysis of trends of plot (a), (c) N accumulated NH_4^+ contents, (d) normalized total nitrogen decays, and (e) percent distributions of the nitrogen species at the end of the trial at *I* = 500 mA.

Fig. 3. Change of the concentrations of **(**a) Cl^- ion (355 mg dm^{-3} of initial Cl^-), (c) ClO_3^- ion, and (d) ClO_4^- ion with electrolysis time for the assays of Fig. 2. (b) Pseudo first-order kinetic analysis for the data of plot (a).

Fig. 4. (a) Time course of terbuthylazine (TBZE) concentration and its pseudo-first-order decay (inset) during the electrochemical oxidation (EO) of 500 cm^3 of a 10 mM Na_2SO_4 solution with 5 mg dm^{-3} herbicide in pure water, using an undivided stirred BDD/Fe tank reactor at 500 mA and 25 ºC. The content of compounds accumulated during this trial is shown in: (b) desethyl-terbuthylazine (DE-TBZE), (c) inorganic N-compounds (N-NH_4^+ and N-NO_3^-) and (d) final acids.

Fig. 5. (a) TBZE content abatement during the paired EO/electrodenitrification of 500 cm^3 of a solution containing 5 mg dm^{-3} herbicide in pure water with 100 mg dm^{-3} NO_3^- + 7.6 mM SO_4^{2-} at pH 4.0, using undivided stirred BDD/Fe or RuO_2/Fe tank reactors at 500 mA and 25 ºC. (b) Accumulated

DE-TBZE concentrations, (c) NO_3^- concentration removal, (d) NH_4^+ accumulated concentrations, (e) normalized total nitrogen decays, and (f) percent distributions of the nitrogen compounds at the end of the trials.

Fig. 6. Influence of pH and current on the time course of (a) TBZE content during the paired EO/electrodenitrification of 500 cm^3 of a solution containing 5 mg dm^{-3} herbicide in pure water with 10 mM Cl^- + 100 mg dm^{-3} NO_3^- + 0.8 mM SO_4^{2-}, using an undivided stirred BDD/Fe tank reactor at 25 ºC. (b) NO_3^- concentrations, (c) normalized total nitrogen decays, (d) percent distribution of the nitrogen species at the end of the trials, (e) active chlorine concentrations, (f) ClO_3^- contents and (g) ClO_4^- concentrations.

Fig. 7. Effect of pH and current under the conditions described in Fig. 6, but using an undivided stirred RuO_2/Fe tank reactor.

Fig. 8. Change of the concentrations of: (a) TBZE, (b) DE-TBZE, (c) NO_3^-, (d) NH_4^+, (e) normalized total nitrogen, (f) Cl^-, (g) ClO_3^- and (h) ClO_4^- during the paired EO/electrodenitrification of 500 cm^3 of the simulated groundwater (10 mM Cl^- + 100 mg dm^{-3} NO_3^- + 0.8 mM SO_4^{2-}) or softened actual groundwater containing 5 mg dm^{-3} herbicide, using 1 BDD anode and 2 Fe cathodes. For comparison, the results for the treatment of actual groundwater without TBZE using 1 Fe cathode are also shown.

Fig. 9. Initial reaction pathway for terbuthylazine degradation in groundwater by EO with a BDD/Fe cell.

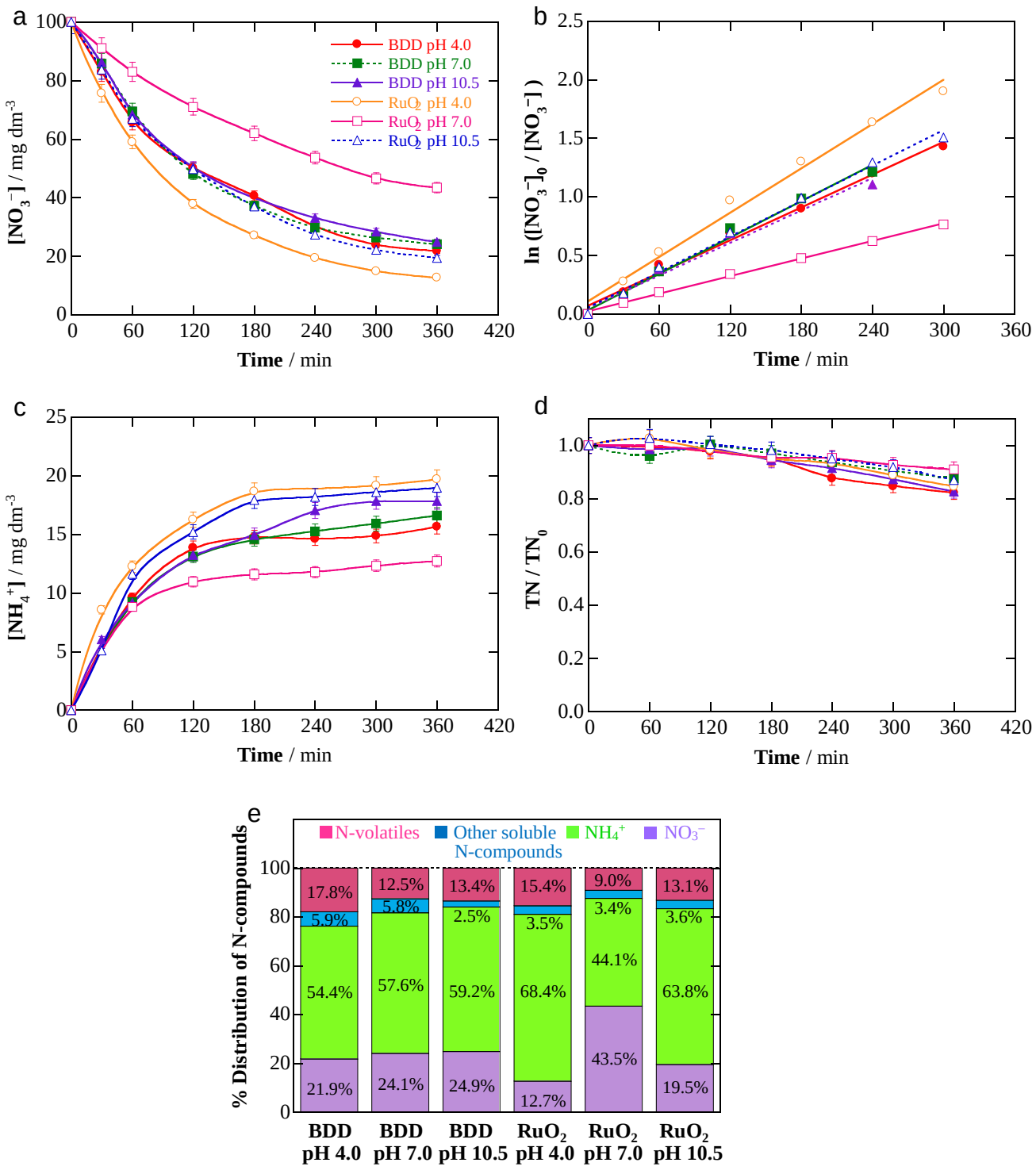
a
b
c
d
e
BDD pH 4.0
BDD pH 7.0
BDD pH 10.5
RuO2 pH 4.0
RuO2 pH 7.0
RuO2 pH 10.5
[NO3−] / mg dm-3
ln ([NO3−]0 / [NO3−])
[NH4+] / mg dm-3
TN / TN0
Time / min
N-volatiles
Other soluble N-compounds
NH4+
NO3−
% Distribution of N-compounds
17.8%
5.9%
54.4%
21.9%
12.5%
5.8%
57.6%
24.1%
13.4%
2.5%
59.2%
24.9%
15.4%
3.5%
68.4%
12.7%
9.0%
3.4%
44.1%
43.5%
13.1%
3.6%
63.8%
19.5%
BDD pH 4.0
BDD pH 7.0
BDD pH 10.5
RuO2 pH 4.0
RuO2 pH 7.0
RuO2 pH 10.5

Fig. 1

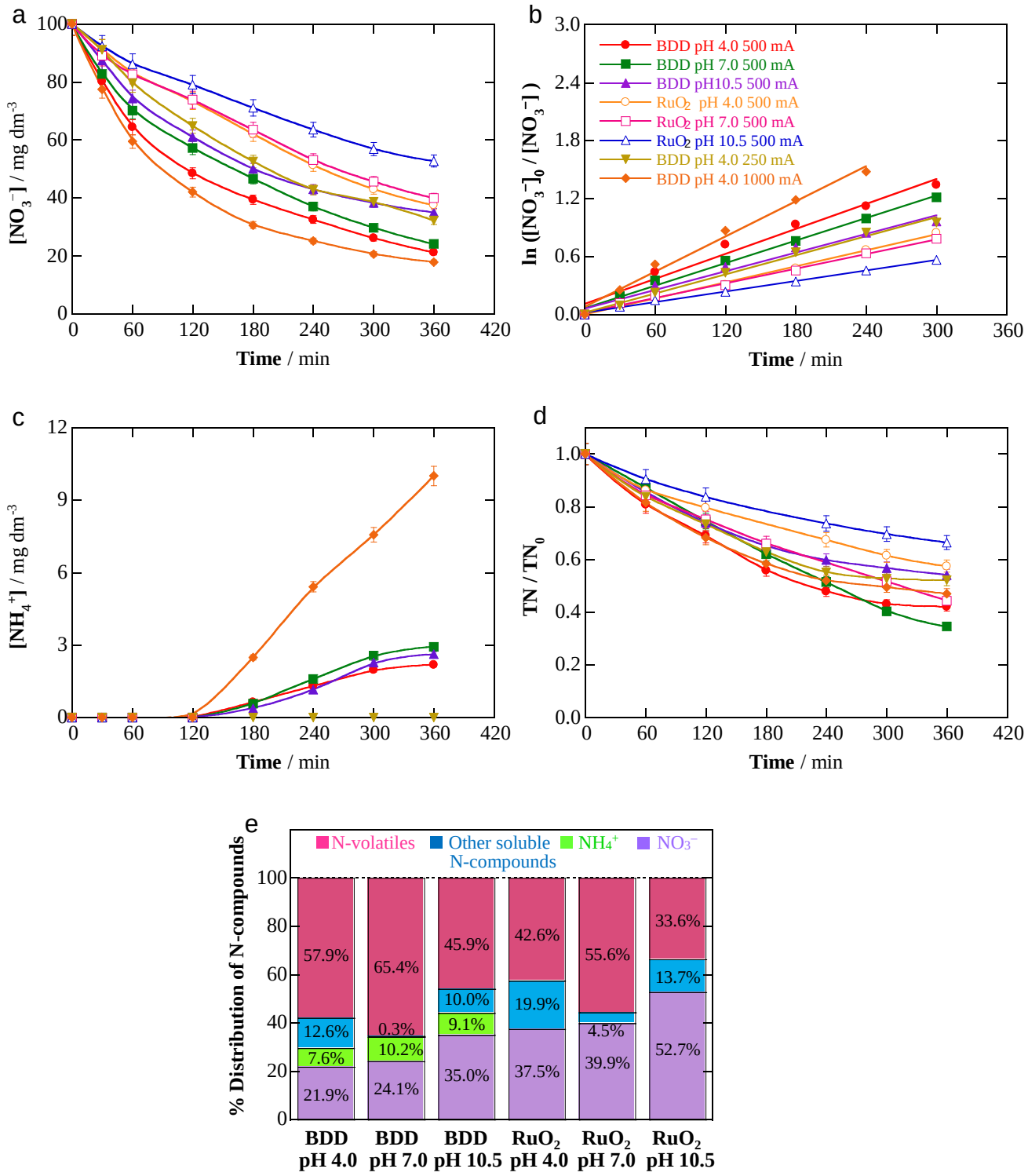
a
b
c
d
e
Time / min
BDD pH 4.0 500 mA
BDD pH 7.0 500 mA
BDD pH10.5 500 mA
RuO2 pH 4.0 500 mA
RuO2 pH 7.0 500 mA
RuO2 pH 10.5 500 mA
BDD pH 4.0 250 mA
BDD pH 4.0 1000 mA
N-volatiles
Other soluble N-compounds
NH4+
NO3−
% Distribution of N-compounds
BDD pH 4.0
BDD pH 7.0
BDD pH 10.5
RuO2 pH 4.0
RuO2 pH 7.0
RuO2 pH 10.5

Fig. 2

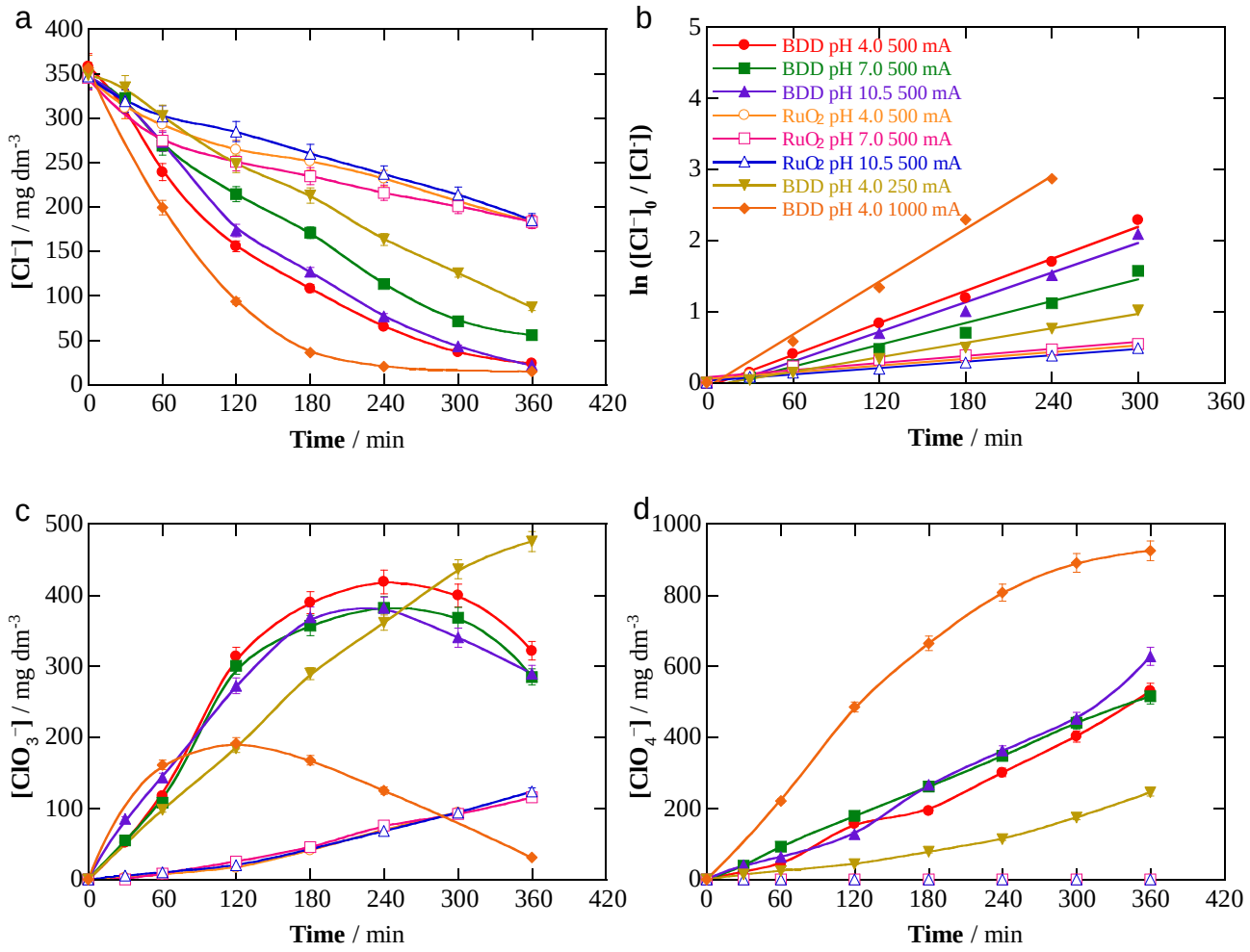
a
b
c
d
[Cl⁻] / mg dm⁻³
ln ([Cl⁻]₀ / [Cl⁻])
[ClO₃⁻] / mg dm⁻³
[ClO₄⁻] / mg dm⁻³
Time / min
BDD pH 4.0 500 mA
BDD pH 7.0 500 mA
BDD pH 10.5 500 mA
RuO2 pH 4.0 500 mA
RuO2 pH 7.0 500 mA
RuO2 pH 10.5 500 mA
BDD pH 4.0 250 mA
BDD pH 4.0 1000 mA

Fig. 3

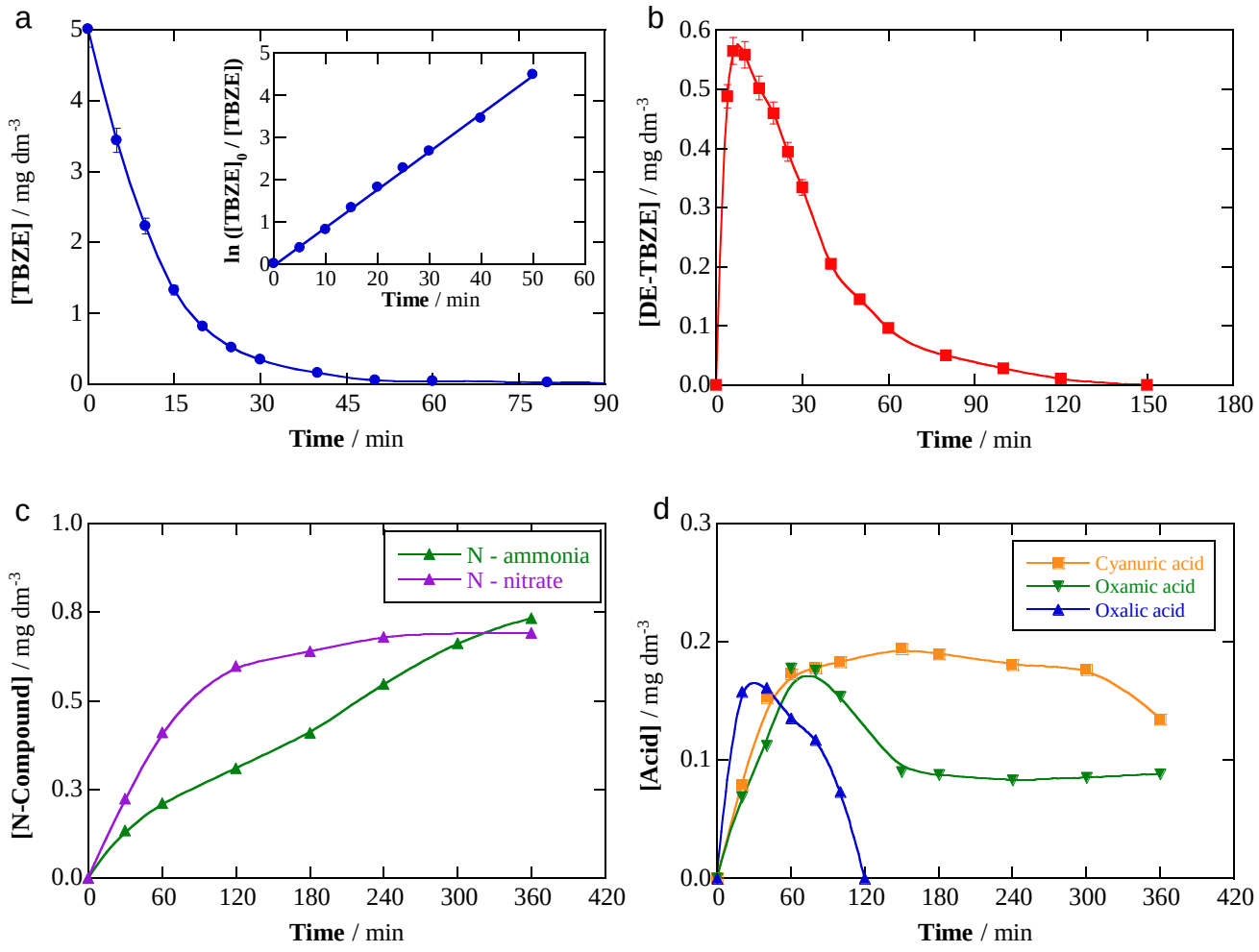
a
[TBZE] / mg dm-3
Time / min
ln ([TBZE]0 / [TBZE])
Time / min
b
[DE-TBZE] / mg dm-3
Time / min
c
[N-Compound] / mg dm-3
N - ammonia
N - nitrate
Time / min
d
[Acid] / mg dm-3
Cyanuric acid
Oxamic acid
Oxalic acid
Time / min

Fig. 4

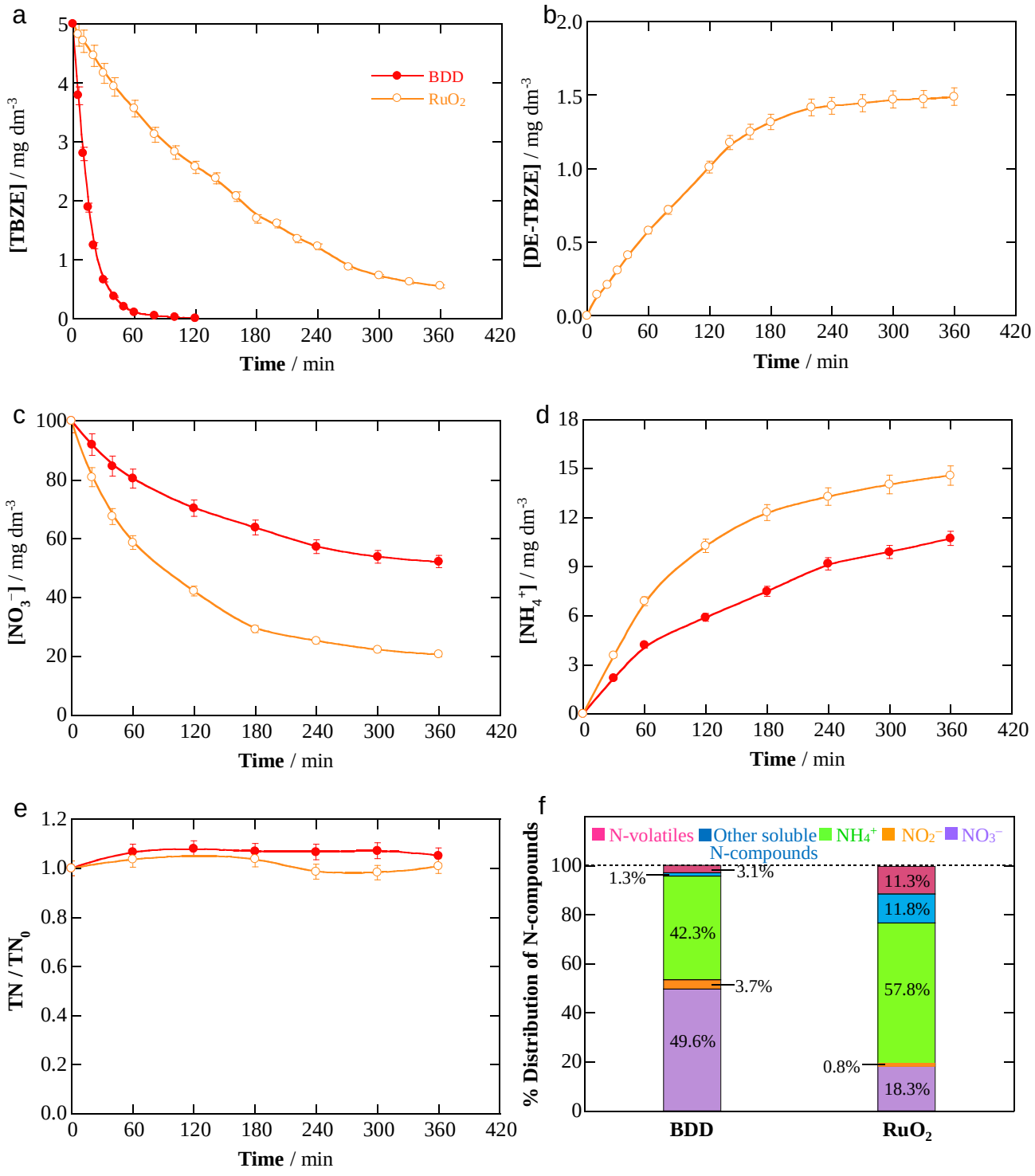
a
[TBZE] / mg dm-3
Time / min
BDD
RuO2
b
[DE-TBZE] / mg dm-3
Time / min
c
[NO3−] / mg dm-3
Time / min
d
[NH4+] / mg dm-3
Time / min
e
TN / TN0
Time / min
f
N-volatiles
Other soluble N-compounds
NH4+
NO2−
NO3−
% Distribution of N-compounds
1.3%
3.1%
42.3%
3.7%
49.6%
11.3%
11.8%
57.8%
0.8%
18.3%
BDD
RuO2

Fig. 5

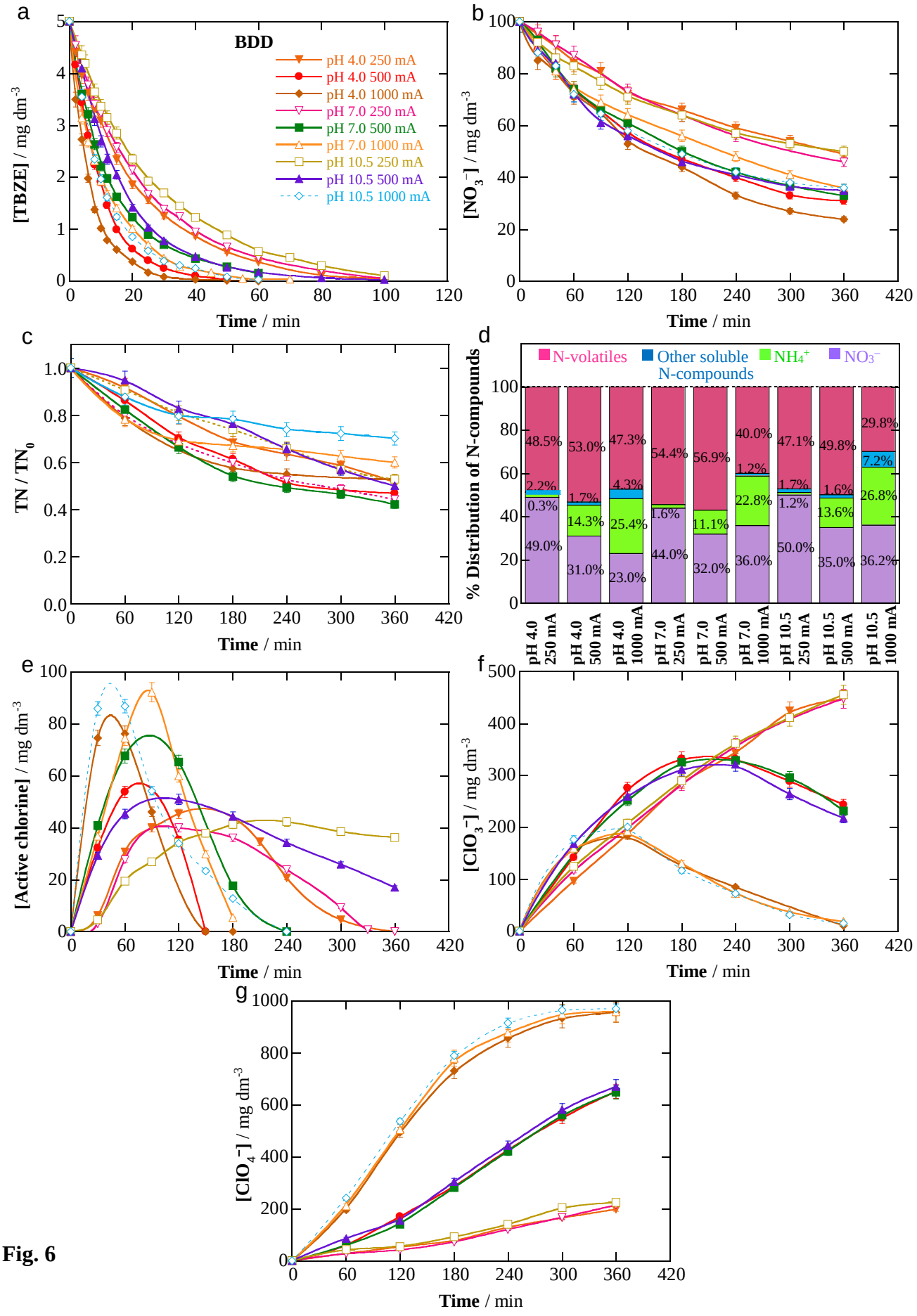
a
BDD
pH 4.0 250 mA
pH 4.0 500 mA
pH 4.0 1000 mA
pH 7.0 250 mA
pH 7.0 500 mA
pH 7.0 1000 mA
pH 10.5 250 mA
pH 10.5 500 mA
pH 10.5 1000 mA
[TBZE] / mg dm-3
Time / min
b
[NO3−] / mg dm-3
Time / min
c
TN / TN0
Time / min
d
N-volatiles
Other soluble N-compounds
NH4+
NO3−
% Distribution of N-compounds
48.5% 2.2% 0.3% 49.0%
53.0% 1.7% 14.3% 31.0%
47.3% 4.3% 25.4% 23.0%
54.4% 1.6% 44.0%
56.9% 11.1% 32.0%
40.0% 1.2% 22.8% 36.0%
47.1% 1.7% 1.2% 50.0%
49.8% 1.6% 13.6% 35.0%
29.8% 7.2% 26.8% 36.2%
pH 4.0 250 mA
pH 4.0 500 mA
pH 4.0 1000 mA
pH 7.0 250 mA
pH 7.0 500 mA
pH 7.0 1000 mA
pH 10.5 250 mA
pH 10.5 500 mA
pH 10.5 1000 mA
e
[Active chlorine] / mg dm-3
Time / min
f
[ClO3−] / mg dm-3
Time / min
g
[ClO4−] / mg dm-3
Time / min

Fig. 6

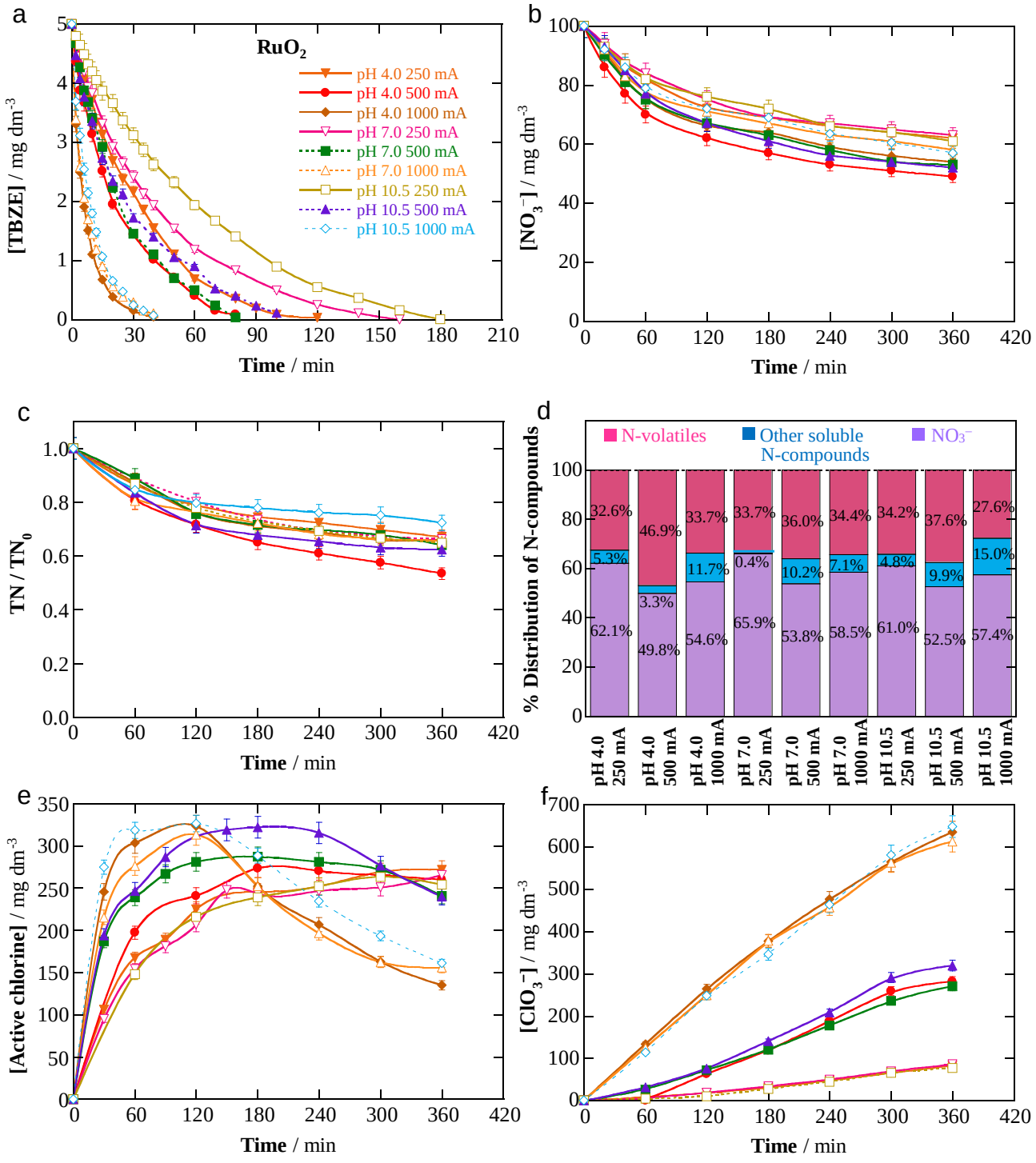
a
RuO2
pH 4.0 250 mA
pH 4.0 500 mA
pH 4.0 1000 mA
pH 7.0 250 mA
pH 7.0 500 mA
pH 7.0 1000 mA
pH 10.5 250 mA
pH 10.5 500 mA
pH 10.5 1000 mA
[TBZE] / mg dm-3
Time / min
b
[NO3−] / mg dm-3
Time / min
c
TN / TN0
Time / min
d
N-volatiles
Other soluble N-compounds
NO3−
% Distribution of N-compounds
32.6% 5.3% 62.1%
46.9% 3.3% 49.8%
33.7% 11.7% 54.6%
33.7% 0.4% 65.9%
36.0% 10.2% 53.8%
34.4% 7.1% 58.5%
34.2% 4.8% 61.0%
37.6% 9.9% 52.5%
27.6% 15.0% 57.4%
pH 4.0 250 mA
pH 4.0 500 mA
pH 4.0 1000 mA
pH 7.0 250 mA
pH 7.0 500 mA
pH 7.0 1000 mA
pH 10.5 250 mA
pH 10.5 500 mA
pH 10.5 1000 mA
e
[Active chlorine] / mg dm-3
Time / min
f
[ClO3−] / mg dm-3
Time / min

Fig. 7

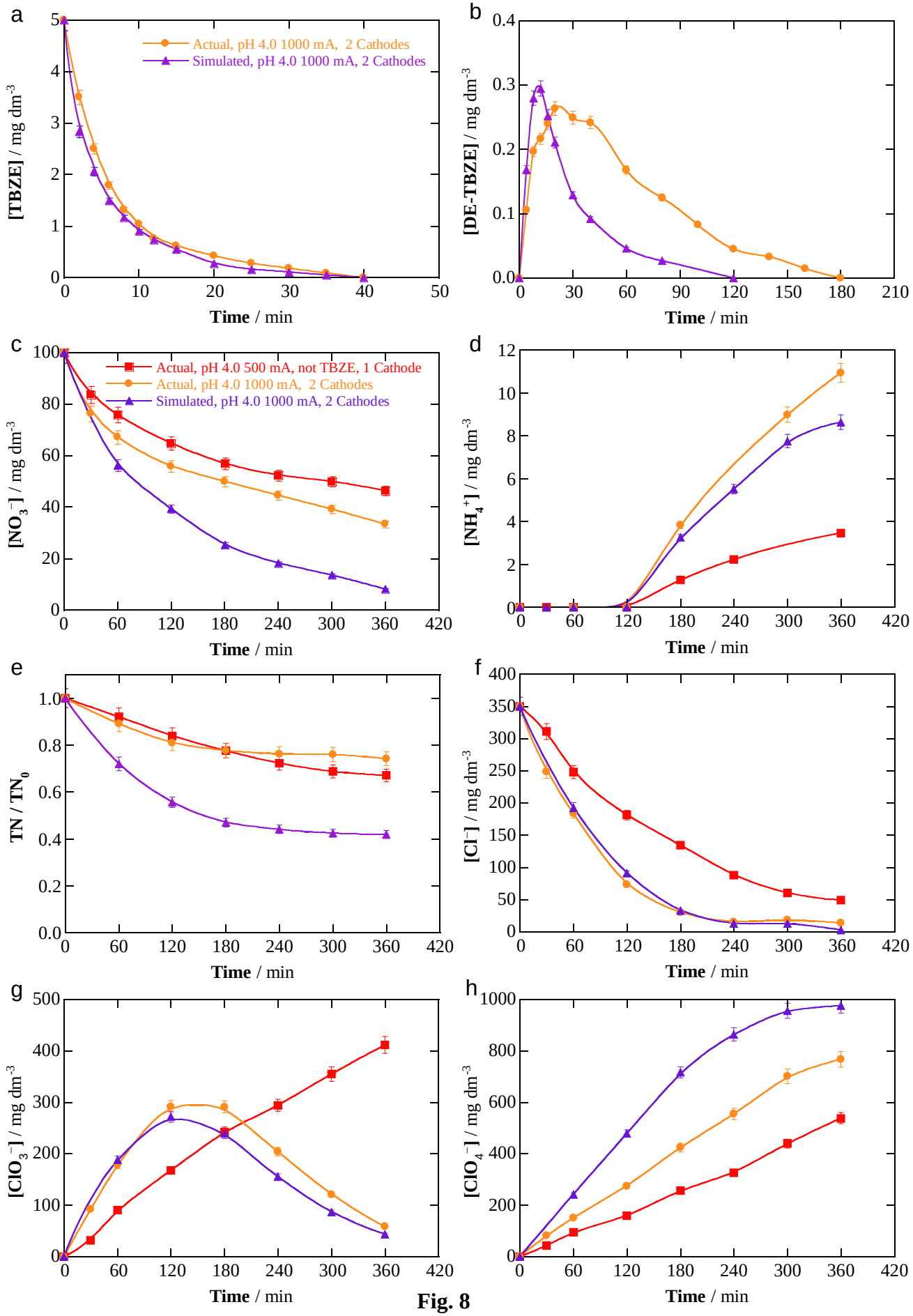
a
Actual, pH 4.0 1000 mA, 2 Cathodes
Simulated, pH 4.0 1000 mA, 2 Cathodes
[TBZE] / mg dm-3
Time / min
b
[DE-TBZE] / mg dm-3
Time / min
c
Actual, pH 4.0 500 mA, not TBZE, 1 Cathode
Actual, pH 4.0 1000 mA, 2 Cathodes
Simulated, pH 4.0 1000 mA, 2 Cathodes
[NO3-] / mg dm-3
Time / min
d
[NH4+] / mg dm-3
Time / min
e
TN / TN0
Time / min
f
[Cl-] / mg dm-3
Time / min
g
[ClO3-] / mg dm-3
Time / min
h
[ClO4-] / mg dm-3
Time / min

Fig. 8

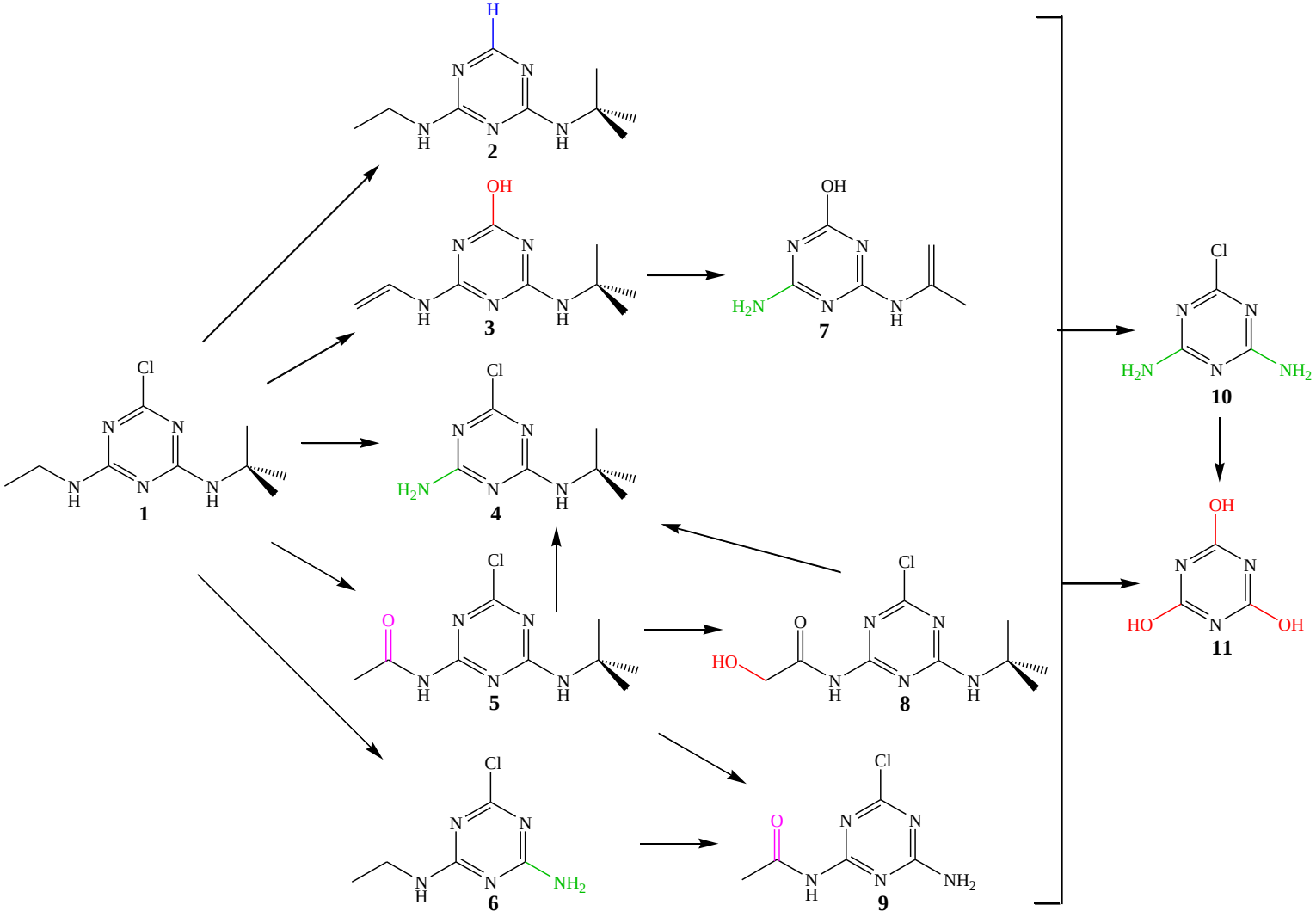

Fig. 9

Table 1

Physicochemical characteristics of the raw groundwater, the softened groundwater after conditioning at pH 4.00 and addition of 5 mg dm^{-3} TBZE, the electrolyzed softened groundwater after 360 min of an EO/electrodenitrification treatment in an undivided stirred BDD/Fe tank reactor at I = 500 mA and 25 ºC, and the same final solution once post-treated with Purolite® A532E ion-exchange resin.

Parameter (units)	Raw groundwater	Softened groundwater	Electrolyzed groundwater	Post-treated groundwater
pH	7.19	4.00	10.20	8.31
Conductivity (mS cm^{-1})	1.72	1.93	1.90	2.02
TC (mg dm^{-3})	50.02	- [a]	- [a]	- [a]
TOC (mg dm^{-3})	1.30	3.74	2.43	2.22
TN (mg dm^{-3})	23.89	23.77	16.76	10.58
NO_3^- (mg dm^{-3})	101.32	99.76	33.43	5.26
NO_2^- (mg dm^{-3})	- [b]	- [b]	2.72	- [b]
Cl^- (mg dm^{-3})	363.26	344.26	42.2	712.31
ClO_3^- (mg dm^{-3})	- [b]	- [b]	58.74	3.24
ClO_4^- (mg dm^{-3})	- [b]	- [b]	766.61	- [b]
SO_4^{2-} (mg dm^{-3})	77.52	357.21	358.56	56.91
Ca^{2+} (mg dm^{-3})	99.59	0.87	0.84	1.31
Mg^{2+} (mg dm^{-3})	26.57	0.55	- [b]	- [b]
K^+ (mg dm^{-3})	9.9	10.47	10.67	11.49
Na^+ (mg dm^{-3})	179.90	389.74	384.53	386.30

[a] Not measured. [b] Not found

Table 2

Pseudo-first-order rate constant for NO_3^-, Cl^- and terbuthylazine decays, alongside the energy consumption at 360 min of electrolysis, for the treatment of 500 cm^3 of simulated groundwater matrices and softened actual groundwater in the absence and presence of herbicide at different pH values and 25 ºC. The assays were made using undivided cells with a BDD or RuO_2 anode and an Fe cathode.

Anode	pH_0 (pH_f)	I / mA	E_{cell} / V	$k(NO_3^-)$ / 10^{-3} min^{-1} (R^2)	$k(Cl^-)$ / 10^{-3} min^{-1} (R^2)	k(TBZE) / 10^{-2} min^{-1} (R^2)	EC / kWh m^{-3}
Simulated groundwater (100 mg dm^{-3} NO_3^- + 7.6 mM SO_4^{2-})							
BDD	4.0 (10.3)	500	8.4	4.7 (0.990)	-	-	50.4
	7.0 (10.7)	500	8.3	5.2 (0.988)	-	-	49.8
	10.5 (10.8)	500	7.5	4.6 (0.981)	-	-	45.0
RuO_2	4.0 (10.1)	500	6.7	6.3 (0.987)	-	-	40.2
	7.0 (11.2)	500	6.5	2.5 (0.997)	-	-	39.0
	10.5 (10.0)	500	6.9	5.0 (0.993)	-	-	41.4
Simulated groundwater (10 mM Cl^- + 100 mg dm^{-3} NO_3^- + 0.8 mM SO_4^{2-})							
BDD	4.0 (10.3)	250	5.4	3.3 (0.991)	3.4 (0.988)	-	16.2
	4.0 (10.2)	500	8.5	4.3 (0.980)	7.5 (0.994)	-	51.0
	7.0 (10.3)	500	8.6	3.9 (0.993)	5.1 (0.981)	-	51.6
	10.5 (10.4)	500	8.0	3.2 (0.980)	7.0 (0.986)	-	48.0
	4.0 (10.7)	1000	13.5	6.1 (0.988)	12.4 (0.993)	-	162.0
RuO_2	4.0 (8.4)	500	7.5	2.8 (0.997)	1.6 (0.985)	-	45.0
	7.0 (9.8)	500	7.5	2.5 (0.995)	1.7 (0.980)	-	45.0
	10.5 (10.0)	500	7.3	1.8 (0.997)	1.5 (0.991)	-	43.8
Simulated groundwater (5.0 mg dm^{-3} TBZE + 10 mM SO_4^{2-})							
BDD	4.0 (4.35)	500	8.3	-	-	9.0 (0.998)	49.8
Simulated groundwater (5.0 mg dm^{-3} TBZE + 100 mg dm^{-3} NO_3^- + 7.6 mM SO_4^{2-})							
BDD	4.0 (9.3)	500	8.0	2.2 (0.981)	-	5.7 (0.988)	48.0
RuO_2	4.0 (10.9)	500	7.5	6.5 (0.989)	-	0.63 (0.994)	45.0
Simulated groundwater *(5.0 mg dm^{-3} TBZE + 10 mM Cl^- + 100 mg dm^{-3} NO_3^- + 0.8 mM SO_4^{2-})*							
BDD	4.0 (10.6)	250	5.8	2.1 (0.984)	-[a]	4.5 (0.997)	17.4
	4.0 (9.9)	500	9.1	3.6 (0.988)	-[a]	9.9 (0.998)	54.6
	4.0 (10.4)	1000	14.7	4.3 (0.993)	-[a]	12.0 (0.993)	176.4
	7.0 (10.6)	250	6.1	2.5 (0.998)	-[a]	4.3 (0.991)	18.3

	7.0 (10.5)	500	10.4	3.3 (0.982)	-[a]	5.6 (0.991)	62.4
	7.0 (10.0)	1000	16.3	2.8 (0.980)	-[a]	7.2 (0.985)	185.6
	10.5 (9.8)	250	6.7	2.1 (0.983)	-[a]	3.6 (0.995)	20.1
	10.5 (10.4)	500	9.2	4.4 (0.981)	-[a]	5.2 (0.993)	55.2
	10.5 (10.0)	1000	14.2	3.6 (0.982)	-[a]	8.0 (0.995)	170.4
BDD[b]	4.0 (10.6)	1000	8.8	6.6 (0.993)	14.0 (0.990)	16.5 (0.982)	105.6
RuO_2	4.0 (9.6)	250	4.4	3.3 (0.986)	-[a]	3.4 (0.988)	13.2
	4.0 (9.7)	500	8.0	5.9 (0.989)	-[a]	4.7 (0.980)	48.0
	4.0 (10.1)	1000	14.2	5.0 (0.991)	-[a]	11.1 (0.993)	170.4
	7.0 (9.8)	250	5.3	3.0 (0.981)	-[a]	2.4 (0.996)	15.4
	7.0 (9.8)	500	8.3	4.8 (0.995)	-[a]	4.1 (0.993)	49.8
	7.0 (9.3)	1000	14.1	4.4 (0.997)	-[a]	9.1 (0.991)	169.2
	10.5 (10.3)	250	4.9	3.3 (0.998)	-[a]	1.8 (0.991)	14.7
	10.5 (10.3)	500	8.9	4.4 (0.995)	-[a]	3.0 (0.992)	53.4
	10.5 (9.5)	1000	13.4	3.9 (0.998)	-[a]	9.8 (0.998)	160.8
Softened actual groundwater							
BDD[c]	4.0 (9.7)	500	7.1	-[e]	5.7 (0.996)	-[a]	42.6
BDD[b,d]	4.0 (10.2)	1000	8.9	-[e]	13.4 (0.997)	15.6 (0.997)	106.8

[a] Not determined. [b] 2 Fe cathodes. [c] Without and [d] with 5.0 mg dm^{-3} TBZE. [e] Nonlinear correlation.

Table 3

Products identified by GC-MS after 60 min of EO/electrodenitrification of 500 cm^3 of solutions with 5.0 mg dm^{-3} terbuthylazine in a simulated matrix at pH 4.0 and 25 ºC using a BDD/Fe cell at 500 mA.

No.	Chemical name	Molecular structure	Column [a]	t_r / min	Fragments [b] *m/z*
1	Terbuthylazine (TBZE)	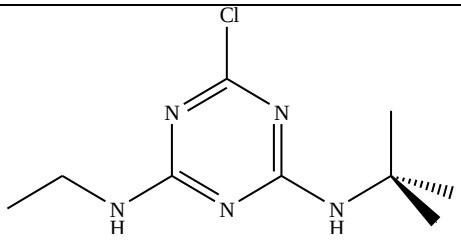	P [c, d] NP [c, d]	40.71 30.73	229 214 **(**- CH_3) 173 (- $C(CH_3)_3$ + H) 158 (173 - CH_3)
2	*N-tert*-butyl-*N'*-[1,3,5]triazine-2,4-diamine[a,b]	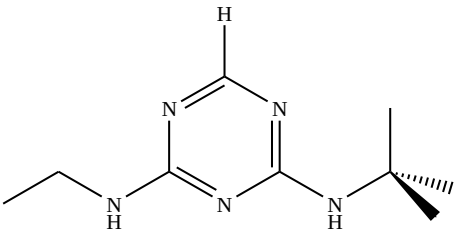	P [c] NP [c, d]	33.93 26.92	195 180 (- CH_3) 139 (- ($C(CH_3)_3$ + H)) / - CH_3-CH_2-NH-C-)
3	4-*tert*buthylamino-6-vinylamino-[1,3,5]triazine-2-ol	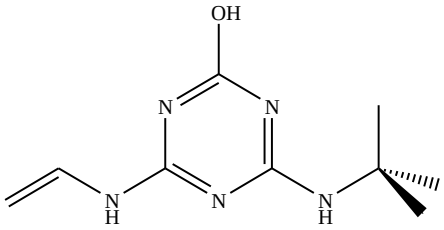	P [d] NP [d]	40.47 29.84	209 194 (- CH_3) 152 (- $C(CH_3)$ / 194 - $C(CH_3)_2$) 125 (152 - $CH=CH_2$)
4	(Desethyl-terbuthylazine), *N-tert*-butyl-6-chloro-[1,3,5]triazine-2,4-diamine (DE-TBZE)	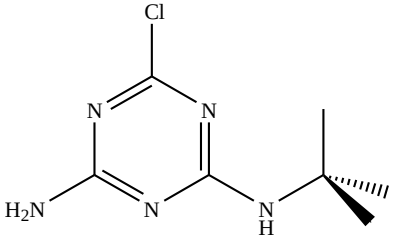	P [c]	43.98	201 186 (- (NH_2 + H)) 145 (- ($C(CH_3)_3$ + H)) 173 (- $C(NH_2)$-) 138 (173 -Cl)
5	*N*-(4-*tert*-butylamino-6-chloro-[1,3,5]triazine-2-yl)-acetamide	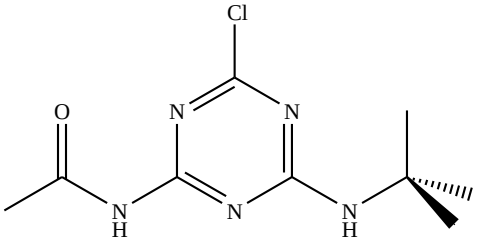	P [c,] NP [d]	45.31 33.23	243 228 (- CH_3) 200 (- (CO-CH_3)) 186 (- $C(CH_3)_3$)
6	6-chloro-*N*-ethyl-[1,3,5]triazine-2,4-diamine	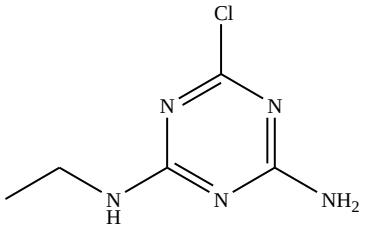	P [c, d] NP [c, d]	47.42 28.36	173 158 (- (NH_2 + H) / - CH_3) 145 (- (CH_2-CH_3 + H)) 110 (145 -Cl)

7	4-amino-6-isopropenylamino-[1,3,5]triazine-2-ol	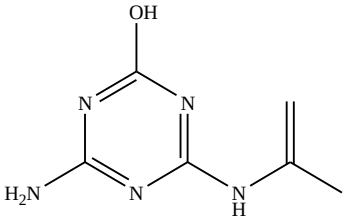	P [d]	36.56	167 152 (- CH_3) 111 (- NH-$C(CH_2)$-CH_3)
8	*N*-(4-*tert*-butylamino-6-chloro-[1,3,5]triazine-2-yl)-2-hydroxy-acetamide	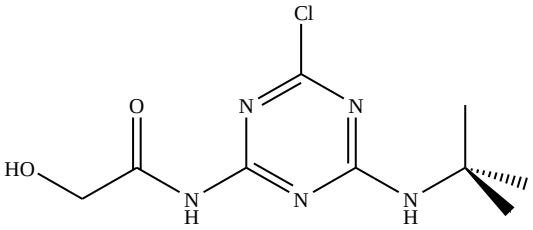	P [c,]	42.60	259 185 (- NH-$C(O)$-CH_2OH) 129(185 – ($C(CH_3)_3$ +H))
9	*N*-(4-amino-6-chloro-[1,3,5]triazine-2-yl)-acetamide	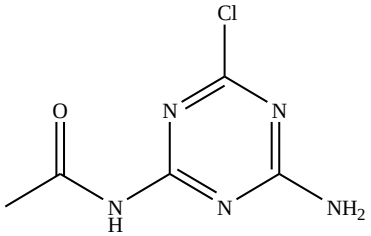	P [c]	45.48	187 172 **(**- CH_3) 145 (- **(**C(O)-CH_3 +H)) 110 (145 - Cl)
10	6-chloro-[1,3,5]triazine-2,4-diamine	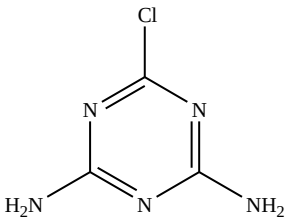	P [d]	41.89	145
11	Cyanuric acid	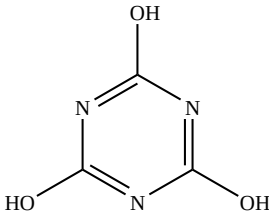	P [c]	30.27	129 115 (- N-) 98 (115 - OH) 87 (129 – (N-C(OH)- + H)) 73 (87 - N-)

[a] P: polar column, NP: Nonpolar column. [b] The mass (*m*) of chlorinated fragments considered the isotope ^{35}Cl. [c] Medium: 100 mg dm^{-3} NO_3^- + 7.6 mM SO_4^{2-}. [d] Medium: 10 mM Cl^- + 100 mg dm^{-3} NO_3^- + 0.8 mM SO_4^{2-}

CReDiT Author statement

Roger Oriol: Conceptualization, Formal analysis, Investigation, Methodology; **Enric Brillas**: Data curation, Formal analysis, Writing-original draft, Writing-review & editing; **Pere L. Cabot**: Funding acquisition, Validation; **José L. Cortina**: Resources, Validation; **I. Sirés**: Conceptualization, Funding acquisition, Project administration, Supervision, Writing-original draft, Writing-review & editing.

Declaration of interests

☒ The authors declare that they have no known competing financial interests or personal relationships that could have appeared to influence the work reported in this paper.

☐The authors declare the following financial interests/personal relationships which may be considered as potential competing interests:

Highlights

- Successful paired electro-oxidation/electrodenitrification of groundwater with Fe cathodes
- Pseudo-first-order kinetics for NO_3^- and terbuthylazine (TBZE) removals with BDD and RuO_2
- NH_4^+ or N-volatiles as main N-products depending on Cl^- content, pH and applied *I*
- Groundwater with BDD/Fe: total TBZE disappearance, sufficient NO_3^- removal (< WHO limit)
- Initial reaction pathway for TBZE degradation: 10 heteroaromatics + oxalic and oxamic acids